PREDICTION OF NACELLE AERODYNAMIC INTERFERENCE
EFFECTS AT LOW SUPERSONIC MACH NUMBERS

Robert M. Kulfan
Boeing Commercial Airplane Company

SUMMARY

A limited study is currently underway to assess the accuracy of analytical predictions of nacelle aerodynamic interference effects at low supersonic speeds by means of test versus theory comparisons. This paper presents a status report of the study.

Comparisons shown include:

- Isolated wing-body lift, drag, and pitching moments

- Isolated nacelle drag and pressure distributions

- Nacelle interference shock-wave patterns and pressure distributions on the wing lower surface

- Nacelle interference effects on wing-body lift, drag, and pitching moments

- Total installed nacelle interference effects on lift, drag and pitching moment.

The comparisons also illustrate effects of nacelle location, nacelle spillage, angle of attack and Mach number on the aerodynamic interference.

The initial results seem to indicate that the methods can satisfactorily predict lift, drag, pitching moment and pressure distributions of installed engine nacelles at low supersonic Mach numbers with mass flow ratios from 0.7 to 1.0 for configurations typical of efficient supersonic cruise airplanes.

1.0 INTRODUCTION

Mutual interference between engine nacelles and the airframe can have an important effect on the aerodynamic efficiency of a supersonic aircraft. Analytical methods exist that allow predicton of these mutual interference effects. A number of systematic analytic studies have been made to obtain an understanding of the design considerations necessary to optimize the favorable aerodynamic interference effects, (refs. 1, 2, 3, 4, 5).

The validation of the necessary design "tools" by means of test-theory comparisons is rather limited (e.g. refs. 3, 4). This is particularly true for the low supersonic speed regime. Additionally, engine spillage effects on aerodynamic interference are relatively unknown.

The National Aeronautics and Space Administration conducted an extensive wind tunnel test program to evaluate aerodynamic performance penalties associated with the propulsion system installation and operation at subsonic through low supersonic speeds. A parallel objective of this test program was to provide an experimental data base of detailed force and pressure measurements for use in systematic evaluations of analytical prediction methods. The results of the NASA experimental test program are reported in references 6 through 8.

A limited study is currently underway to assess the accuracy of the theoretical predictions of supersonic engine-airframe interference effects. The objective of this paper is to present the initial results of this study.

The NASA wind tunnel model geometry and test conditions are summarized in Section 2.0. The prediction methods being evaluated in this study are discussed in Section 3.0. A brief description of wing-nacelle aerodynamic interactions is given in Section 4.0.

Isolated wing plus body comparisons and isolated nacelle test versus theory comparisons are presented in Sections 5.0 and 6.0, respectively.

Nacelle interference pressures acting on the wing lower surface are shown in Section 7.0. Section 8.0 contains interference lift, drag and pitching moment comparisons.

The procedure that was used to calculate spillage effects on nacelle interference is described in Section 9.0. Comparisons of predicted spillage aerodynamic effects are presented in Section 10.0.

2.0 MODEL GEOMETRY AND TEST CONDITIONS

The NASA experimental program was conducted in the Ames 11- by 11-foot wind tunnel. The basic features of the nacelle-airframe interference model are shown in figure 1. The wing-body configuration is a .024 scale model of the 1971 SST. The wing-body was sting mounted with a six-component internal strain-gage balance. The left-hand wing had 126 static pressure orifices - 95 on the lower surface and 31 on the upper surface. The orifice locations are shown in figure 2. Two different nacelle geometries were tested. One set of nacelles had sharp inlets. The second set of nacelles had a slightly blunt inlet lip shape. The investigations reported in this paper concern only the sharp lip nacelles.

The tested nacelle shape is a simplified and slightly oversize representation of a typical supersonic nacelle installation, as shown in

figure 3. The nacelles were located approximately 1.2 inlet diameters below the wing chord plane. This resulted in a gap between the nacelles and the wing lower surface that does not exist in an actual nacelle/airframe installation.

The four individual nacelles were supported below the wing-body model on individual flow-through-stings. The two left-hand side nacelles (looking upstream) were pressure instrumented. The two right-hand side nacelles were mounted individually on separate six-component internal strain-gage balances. The pressure instrumented nacelles had 40 static-pressure orifices as shown in figure 2.

The six-component force balances used to support the right-hand nacelles were housed in the thickness of each nacelle. A two-shell flow-through balance located in each nacelle used four instrumented flexures located 90 deg. apart at two axial locations. The nacelle balances measured the aerodynamic forces on the external surface of the nacelle, plus the forces on a small portion of the internal duct near the inlet. The wind tunnel data corrections included removal of the estimated skin friction drag on this internal duct area.

The nacelle support system provided the flexibility of positioning the nacelles vertical, streamwise, and spanwise, relative to the wing-body combination and to each other. The range of achievable nacelle locations is indicated in figure 1. The support system also provided for independent control and measurement of mass flow through each nacelle by means of a mass-flow control plug and appropriate pressure instrumentation.

The test configurations included:

- Isolated wing-body

- Isolated nacelle

- Four nacelles in various relative positions

- Wing-body plus nacelles in various locations

The test data included:

- Wing-body lift (C_L), drag (C_D) and pitching moment (C_M) data

- Wing pressure measurements

- Lift, drag and pitching moment measurements of the individual inboard and outboard nacelles

- Nacelle surface pressures

These tested configurations provided the following measurements of isolated and interference data:

Isolated wing-body data -- measurements on wing-body without the nacelles present.

- Isolated nacelle data -- measurements on a singly tested nacelle.

- Mutual nacelle interference -- difference in nacelle measurements with and without the other nacelles present.

  Nacelle interference on wing-body -- difference in wing-body measurements with and without the other nacelles present.

  Wing-body interference on the nacelles -- difference in nacelle measurements with and without the wing-body present.

  Total wing-body plus nacelle data -- sum of wing-body data plus nacelle data.

  Spillage interference -- difference in measurements on identical configurations with the nacelles spilling according to a specific controlled mass flow ratio (MFR), and the corresponding data obtained without spillage.

The test conditions included:

Mach Number: 0.90, 0.98, 1.1, 1.15, 1.2, 1.3, 1.4

Angle of Attack: α = 0 to 6 deg.

Mass flow ratio: MFR = 0.6 to 1.0

All configurations were tested at the primary Mach numbers of 0.9, 1.15, 1.4. Some selected configurations were also tested at the remaining Mach numbers. Only a few configurations were tested at angles of attack different than zero. Configurations with spillage were tested only at zero angle of attack.

The model angle of attack was measured relative to a wing reference plane. At zero angle of attack, the model actually experiences significant negative lift.

Staggered and non-staggered arrangements were tested at six different nacelle stations and three different spanwise locations as shown in figure 4. In this paper only the "no-stagger" configuration results are presented as the staggered nacelle analyses are only currently underway.

Complete descriptions of the wind tunnel model, test conditions and available test data are given in reference 8.

3.0 PREDICTION METHODS

The aerodynamic force and moment predictions for the study reported herein have been made using the system of aerodynamic design and analysis programs described in reference 9. The aerodynamic force coefficients for a specified configuration are built up through superposition.

174

The drag prediction, as summarized in figure 5, includes:

- Skin friction drag, C_{D_F}, calculated using flat plate turbulent flow theory.

- Volume wave drag, C_{D_W}, -- calculated either by a far-field wave drag program (supersonic area rule) or by a near-field (surface pressure integration method) program.

  Drag-due-to-lift, C_{D_L}, which includes induced drag as well as wave-drag-due-to-lift -- calculated by a near-field analysis program.

The near-field force calculations are obtained by integration of the surface pressures (volume or lifting pressures) over each component of the configuration being analyzed. The surface pressures include the isolated component pressures plus the interference pressures acting on each component due to the other components of the configuration.

The nacelle pressure fields imposed on the surface of the wing can be calculated by either the "wrap" method or the "glance" method summarized in figure 6.

In the "wrap" method, the nacelle pressure fields and accompanying shock waves "wrap" around adjacent nacelles. In application, the pressure field generated by one nacelle is allowed to pass through another nacelle as if it were transparent. This is also the approach inherent in the far-field wave drag calculations.

In the "glance" method the pressure fields generated by one nacelle "glance" away from the wing when encountering adjacent nacelles. In application, the nacelle generated flow field is terminated on encountering another nacelle.

One of the objectives of the current study is to determine which of these methods is more nearly correct.

4.0 WING-BODY AND NACELLE INTERACTIONS

At supersonic speeds, the mutual interactions of the wing-body and the nacelles can produce significant interference effects. The nacelle installed drag is usually defined to include the drag of the isolated nacelles plus net effects of the nacelle pressure field acting on the wing-body as well as the effect of the wing-body pressure field acting on the nacelles.

Typically, the nacelle installed drag, as shown in figure 7, is calculated as the sum of the friction drag of the nacelles, the net wave drag, and the lift interference effects.

The net nacelle wave drag includes:

- Nacelle pressure drag
- Nacelle pressures acting on the wing-body volume or thickness

    The wing-body thickness pressures acting on the nacelles
- Mutual nacelle interference

The mutual nacelle interference consists of the effect of the pressure field of a nacelle acting directly on the other nacelles plus the effect of the pressure field reflecting off the wing surface back onto the nacelles.

The lift interference consists of three items:

- The nacelle pressures reflecting off the wing produce an interference lift, ΔC_L. Because of the interference lift, the wing-body incidence required to produce a specified total lift is reduced. This results in a reduction in the wing-body drag due to lift.

    The nacelle pressures acting on mean lifting surface produce a drag or thrust force.
- The wing lifting pressures produce a buoyancy force on the nacelles.

The net nacelle drag is therefore dependent not only on flight conditions and the shape of the nacelles but also on the shape and location of adjacent components of the airplane.

The near field methods described in the previous section calculate each of these contributions to the total nacelle installed drag. The NASA nacelle/airframe interference test described in Section 2 provides an extensive data base of experimentally determined measurements of these contributions to the total nacelle installed drag.

In the sections that follow, test versus theory comparisons provide an indication of the accuracy of the theoretical predictions of the various lift, drag, and pitching moment components with and without spillage.

5.0   ISOLATED WING-BODY COMPARISONS

Figures 8 through 14 contain comparisons of the predicted aerodynamic characteristics of the isolated wing-body configuration.

Drag predictions at zero-lift were made using both the far-field (area-rule) and near-field methods. The drag predictions for this wing-body configuration using the far-field theory wave drag estimates agree very well

with the test data. The near-field theory appears to slightly overestimate the wing-body zero-lift wave drag.

The predicted drag polars are shown in figures 9 and 10 for Mach 1.4 and 1.15, respectively. The near-field zero-lift wave drag estimates were used in these predictions. The main difference between the theoretical and experimental drag polars is the overestimated drag at zero lift. The predicted and experimental polar shapes are nearly the same.

The theoretical lift and pitching moment curves are compared with test data in figures 11 and 12. The theoretical lift curves agree very well with the test data.

The zero-lift pitching moment predictions agree fairly well with the test data. The differences in the slopes of the pitching moment curves indicate that theory predicts the aerodynamic center too far aft.

Figures 13 and 14 summarize the wing-body lift and pitching moment characteristics from subsonic through low supersonic Mach numbers. These figures also contain test data obtained by Boeing on the same model prior to the NASA nacelle-airframe interference test program. The subsonic predictions shown in the figures were obtained by a Boeing in-house aerodynamic influence coefficient method.

The good agreement between the theoretical and experimental drag polars and lift curves indicates that the theory should predict the reductions in wing-body drag-due-to-lift associated with the nacelle interference lift (described in section 4.0).

6.0   ISOLATED NACELLE COMPARISONS

Theoretical predictions of the surface pressure distributions and zero-lift drag of the isolated nacelle are compared with the test data shown in figure 15.

Nacelle wave drag estimates were made using both the far-field and near-field methods. The theoretical predictions agree with the test results at Mach 1.3 and 1.4. The near-field estimates are slightly better than the far-field estimates. Theory overestimates the nacelle drag at Mach 1.2 and below.

The nacelle pressure distribution shown in figure 15 at Mach 1.4 closely matches the test data. At Mach 1.15, theory overestimates the expansion (i.e., negative) pressures on the nacelle boattail. This leads to the overestimation of drag at the lower supersonic Mach numbers. The pressure at the first station at both Mach numbers is less than theory. This is probably due to nacelles actually spilling a small amount of flow at the test conditions.

The near-field method has been used for wave drag predictions in the remainder of the analyses presented in this paper.

7.0 NACELLE INTERFERENCE PRESSURES ON THE WING

Theoretical nacelle shock wave patterns and interference pressures on the wing are compared with test data for one of the aft nacelle locations in Figures 16 and 17.

The experimental interference pressures were obtained as the difference in the wing lower surface pressures with and without the nacelles present.

The interference pressures were calculated by both the "wrap" method and "glance" method described in section 3.0.

The predicted nacelle bow shock locations agree well with the experimental shock locations as indicated by a sudden "jump" in interference pressures, c_{P_I}, from zero to some large positive value.

The interference pressures predicted by the "glance" method agree reasonably well with the experimental data. The theoretical bow shock strength is larger than indicated by the test data. This may be the result of a shock-boundary layer interaction softening this initial sudden pressure rise.

The additional pressure peaks predicted by the "wrap" method are not evident in the test data in either figures 16 or 17. These and similar results obtained, with the nacelles located in different streamwise locations below the wing, indicate that the "glance" method of nacelle pressure field superposition is more realistic than the "wrap" method. Consequently, all of the remaining results to be shown in this paper were obtained by the "glance" method.

Figures 18 and 19 contain comparisons of predicted shock wave patterns and interference pressure fields with test data for a forward nacelle location in which the outboard nacelle is near the wing leading edge. In this nacelle arrangement, the wing experiences not only the bow shocks from the nacelles, but also aft shocks. The aft shocks arise from the flow compression at the aft end of the nacelle where the flow-through-sting enters the nacelle shell.

The predicted and measured interference pressures for this wing-body-nacelle arrangement agree quite well except in local areas near the aft shock and also at the most outboard station.

In Reference 10 it is shown that flow across a glancing shock wave, in which the flow is deflected in the plane of the wing, will separate if the pressure rise across the shock wave exceeds 50%. Furthermore, it is shown that a local negative pressure field on the wing can amplify the pressure rise across a shock wave.

The calculated pressure rises across the nacelle bow shocks shown in Figures 18 and 19 are in the order of 25 to 30 percent. This should not cause separation. Indeed, the experimental bow shock data give no indication of separation.

The aft shock waves from the nacelle are much stronger because of the large boattail angle at the aft end of the nacelle. Furthermore, the nacelle area reduction along the boattail produces theoretically large negative expansion pressure just upstream of the aft shock waves. This local negative pressure field further amplifies the strength of the already strong aft shocks. Consequently, the pressure rise across the aft shocks varies from 60 percent to 100 percent across the wing. Thus, boundary layer separation is most certain to occur in the area of the aft shocks. The differences in the experimental and theoretical pressures near the aft shocks is probably due to shock induced boundary layer separation.

These results demonstrate the importance of limiting the strength of nacelle-created shock waves likely to interact with a wing, particularly in areas of local negative pressures.

8.0 INTERFERENCE LIFT, DRAG, AND PITCHING MOMENT

Comparisons are made in Figures 20 and 21 between calculated nacelle contributions to lift, drag, and pitching moment with the corresponding test data.

The drag comparisons include the nacelle interference on the wing-body as well as the total nacelle installed drag. The theoretical drag predictions agree well with the test data. The nacelle interference on the wing-body is favorable and increases with lift coefficient. This is primarily due to the reduction in wing-body drag-due-to-lift associated with the nacelle interference lift.

Theoretical interference lift and pitching moment increments are calculated from the nacelle interference pressure fields (discussed in the previous section) acting on the wing lower surface. The experimental lift and pitching moment data indicate that the nacelles also experience a change in lift and hence pitching moment when located in the wing lower surface pressure field. The effect of wing-body pressures on nacelle lift is not considered in the theoretical calculations.

The measured interference lift increment increases with angle of attack. The theoretical interference lift calculations shown in Figures 20 and 21 were made at a constant local Mach number equal to the free-stream Mach number. Slender body theory estimates were subsequently made to explore the effect of local Mach number on interference lift. The results of these slender body theory estimates are shown in Figure 22.

A negative pressure field in the area of the nacelles, corresponding to a local Mach number greater than free stream, reduces the interference lift. Conversely, a positive pressure field, or lower local Mach number, enhances the interference lift. The effect of the local pressure field on the interference lift is seen to be greatest at the very low supersonic Mach numbers. The calculated effects of local pressure field on interference lift are consistent with the experimental results shown in Figures 20 and 21.

As a result of the favorable interference effects, the total nacelle drag is less than friction drag at the higher lift coefficients for the analyzed configuration arrangement.

The effect of nacelle location on aerodynamic interference is shown in Figures 23 and 24. Nacelle location is seen to have a powerful effect on the nacelle interference. At the aft nacelle locations, both the interference of the nacelles on the wing-body and the wing-body on the nacelles are favorable. The nacelles in the aft locations produce a substantial level of favorable interference. As the nacelles are moved forward, both of these interference components become unfavorable. This results in considerable net unfavorable interference. The predicted interference effects agree reasonably well with the test data, but become less accurate at the most forward location, where the outboard nacelle moves in front of the wing leading edge.

9.0 SPILLAGE INTERFERENCE CALCULATION PROCEDURE

The results that have been presented in the sections thus far correspond to engine operation without spillage (i.e., mass flow = 1.0). The effects of nacelle spillage (mass flow ratios as low as 0.7) on the interference forces were also investigated in the NASA nacelle-airframe interference test program. Experimental measurements, however, were only obtained at zero angle of attack. As previously mentioned, the wing-body produces considerable negative lift at this attitude.

The mass flow through each nacelle was varied by a control plug in the corresponding flow-through-sting. At supersonic speeds a normal shock forms in front of the nacelle and moves progressively upstream as the mass-flow ratio through the nacelle is reduced.

To calculate spillage effects on the nacelle pressure distribution, the capture streamtube that separates the flow into the inlet from the flow that spills around the inlet is replaced by a solid surface in the mathematical analyses. A simple approach was used in this study to calculate the inlet streamtube shape for spillage behind a normal shock. The method developed by Moeckel (Ref. 11) was used to calculate both the distance of the normal shock forward of the spilling nacelle and the capture streamtube radius at the normal shock. The shape of the capture streamtube was then represented as shown in Figure 25 by a simple polynomial equation. The calculated streamtube shape grows with zero initial slope ($dr/dx = 0$) at the normal shock to match the inlet radius at the nose of the nacelle.

The presence of the capture streamtube changes the pressure distribution over the nacelle. Relative to a non-spilling nacelle, a large expansion occurs at the lip of the nacelle due to the capture streamtube shape at the inlet. This decreases the pressure near the front of the nacelle, thereby reducing the isolated nacelle drag. The isolated nacelle drag reduction is typically called "lip suction".

180

The presence of the capture streamtube changes the interference effects associated with the nacelle pressures acting on the wing-body, as well as on the isolated nacelle and the adjacent nacelles. The capture streamtube does not support a force across its surface. Consequently, in the analyses, only the pressures acting on the nacelle surface contribute directly to drag on the nacelle. Hence, the wing-body interference acting on the nacelles is unchanged by spillage.

10 SPILLAGE EFFECTS ON AERODYNAMIC INTERFERENCE

Streamtube shapes calculated by the method described in the previous section are shown in figures 26 and 27 for a range of mass flow ratios at Mach 1.4 and 1.15, respectively. The calculated shapes indicate rather large changes in the streamtube area occur over short distances relative to the smooth shape of the nacelle.

Figures 28 and 29 contain comparisons of predicted and measured isolated nacelle pressure distributions for different amounts of spillage. Reductions in mass flow ratio cause a decrease in local pressures on the forward section of the nacelle. The experimental pressure reduction is greater than predicted by the theory particularly at the lowest mass flow ratio (i.e., greatest spillage). This is probably because the theoretical analysis treats the capture streamtube as a solid shape in a supersonic flow field, whereas the actual nacelle experiences a complicated mixed subsonic-supersonic flow field.

The experimental data in Figure 30 show large reductions in isolated nacelle drag associated with the reduced nose pressures.

Slender body theory estimates of the effect of spillage on interference lift are shown in Figure 31. The slender body theory calculations of interference lift depend only on the net area change of the capture streamtube and not the shape. The trends predicted by the slender body theory estimates agree well with the test data.

Calculated shock wave patterns and nacelle pressure distributions on the wing are compared with test data for the nacelles with and without spillage at Mach 1.4 and 1.15 in Figures 32 and 33, respectively. These calculations were made with the streamtube geometries shown in Figure 26.

The predicted effect of spillage on nacelle bow-shock locations agrees with the test data. The predicted effects of spillage on the interference pressures on the wing are in fair agreement with the test results. The corresponding interference lift and pitching moment data are shown in Figure 34. Spillage is seen to have a rather large effect on the interference lift.

Figure 35 contains comparisons of calculated nacelle interference drag with test data for different mass flow ratios (i.e., amounts of spillage). The drag of the isolated nacelle, measured at the average mass flow for the

nacelles at each nominal test condition, was removed from the corresponding measured total wing-body-nacelle drag. Similarly the theoretical interference drag predictions do not include the calculated isolated nacelle drag.

The interference of the nacelle pressure field acting on the wing-body produces nearly all of the large favorable interference for this configuration arrangement. Increased nacelle spillage, which corresponds to reduced engine mass flow, has only a small effect on the net interference drag at a fixed angle of attack. For example, a more favorable interference drag increment of 2 counts (ΔC_D = -.0002) is indicated relative to the no-spilling condition for a mass flow ratio of 0.6. The test data, which includes only the nacelle interference on the wing-body, agree quite well with the predictions.

As previously mentioned, nacelle spillage has a rather large effect on the interference lift. Hence, the effects of spillage on net wing-body plus nacelle interference should become more significant when comparisons are made at constant total lift. Figure 35 contains predictions of the net wing-body plus nacelle interference variations with lift coefficient for different amounts of spillage. The favorable interference indeed becomes greater as lift is increased. For example, the nacelles with a mass flow ratio of 0.6 are predicted to produce a favorable interference drag increment of approximately 7 counts (ΔC_D = -.0007) relative to the nacelles without spillage at a lift coefficient of 0.2.

The combined effects of the increased favorable interference at lifting conditions (Fig. 35) plus reduced isolated nacelle drag (Fig. 30) can result in a total nacelle installed drag less than zero. This occurs, for example, for lift coefficients greater than 0.12 for an engine mass flow ratio of 0.6 (i.e., 40% spillage) at Mach 1.4. This is the approximate mass flow ratio of a supersonic inlet (Mach 2.4 to 2.7) operating at transonic speeds.

11.0 CONCLUDING REMARKS

"No-Spillage" Conclusions:

. Far-field and near-field methods adequately predict wing plus body aerodynamic characteristics.

. Far-field and near-field predictions of the isolated nacelle drag are good at Mach 1.4. The drag predictions at Mach 1.15 are higher than the test results because of an overestimate of the nacelle boattail pressures.

. The "glance" method of nacelle pressure field superposition is more accurate than the "wrap" method.

. The locations of nacelle shocks are predicted accurately by the theory.

Predictions of nacelle interference pressures on the wing are good except in local areas near strong shocks where separation occurs.

Predictions of Mach number, nacelle location and angle of attack on nacelle aerodynamic interference are good, but become less accurate as the nacelles are moved forward of the wing leading edge.

. With the nacelles located aft near the wing trailing edge, the favorable interference effects of the nacelle on the wing-body become increasingly large as C_L increases. The net installed drag, both measured and calculated, was less than skin friction drag.

"With Spillage" - Conclusions

. The analysis method developed in the study does not properly account for spillage effects on the isolated nacelle pressure distribution near the lip. Consequently, the method overpredicts the drag of the isolated nacelle with spillage.

The method predicts the forward movement of the nacelle bow shocks on the wing due to spillage.

The method adequately predicted spillage interference effects on lift, drag and pitching moment at zero angle of attack and Mach = 1.4.

The predicted spillage interference effects are favorable and improve with lift coefficient. With spillage, the nacelle installed drag can be less than zero due to the reduction in isolated nacelle drag, plus the increased favorable lift interference.

These initial results seem to indicate that satisfactory methods are available to predict interference lift, drag, pitching moment and pressure distributions of intalled engine nacelles at Mach 1.15 and 1.4 with mass flow ratios from 0.7 to 1.0 for configurations typical of efficient supersonic cruise airplanes.

REFERENCES

(1) Swan, W. C.: Aerodynamics of Powerplant Installation, Part II,
     AGARDograph 103, October 1965

(2) Nichols, M. R.: Aerodynamics of Airframe-Engine Integration of
     Supersonic Aircraft, NASA TND-3390, 1966

(3) Sigalla, A; Hallstaff, T. H.: Aerodynamics of Powerplant Installation on
     Supersonic Aircraft, Journal of Aircraft, July-August 1967, pp 273-277

(4) Kane, E. J.; and Middleton, W. D.: Considerations of Aerodynamic
     Interference in Supersonic Airplane Design, AGARD Conference on
     Aerodynamic Interference, Proceedings No. 71, paper 3, September 1970

(5) Bencze, D. P.: Nacelle-Airframe Interference at Low Supersonic Mach
     Numbers, AIAA Paper No. 72-1113, November 1972

(6) Bencze, D. P.: Wind Tunnel Investigation of Nacelle-Airframe
     Interference at Mach Numbers of 0.90 to 1.4 - Data Report - Force Data,
     NASA TM X-62, 489, 1976

(7) Bencze, D. P.: Wind Tunnel Investigation of Nacelle - Airframe
     Interference at Mach Numbers of 0.9 to 1.4 - Data Report - Pressure
     Data, Volume I - NASA TM X-73, 149, Volume II - NASA TM X-73, 088, 1976

(8) Bencze, D. P.: Experimental Evaluation of Nacelle-Airframe Interference
     Forces and Pressures at Mach Numbers of 0.9 to 1.4, NASA TM X-3321,
     March 1977

(9) Middleton, W. D.; Lundry, J. L.; and Coleman, R. G.: A Computational
     System for Aerodynamic Design and Analysis of Supersonic Aircraft, Part
     2 - User's Manual, NASA CR-2716, August 1976

(10) Kulfan, R. M.; Sigalla, A.: Real Flow Limitations in Supersonic Airplane
     Design, Journal of Aircraft, Vol 16, No. 10, pp 645-658, October 1979

(11) Moeckel, W. E.: Approximate Method for Predicting Form and Location
     of Detached Shock Waves Ahead of Plane or Axially Symmetric Bodies,
     NACA TN 1921, June 1949

WING-BODY

- STING MOUNTED
- SIX-COMPONENT INTERNAL BALANCE
- WING UPPER AND LOWER SURFACE PRESSURES

NACELLES

- INDIVIDUAL FLOW-THROUGH STINGS
- TRANSLATE: VERTICAL, STREAMWISE, SPANWISE
- PITCH WITH WING-BODY
- VARIABLE MASS FLOW
- INTERNAL SIX-COMPONENT BALANCES (RIGHT PAIR)
- NACELLE SURFACE PRESSURES (LEFT PAIR)

AVAILABLE POSITIONS
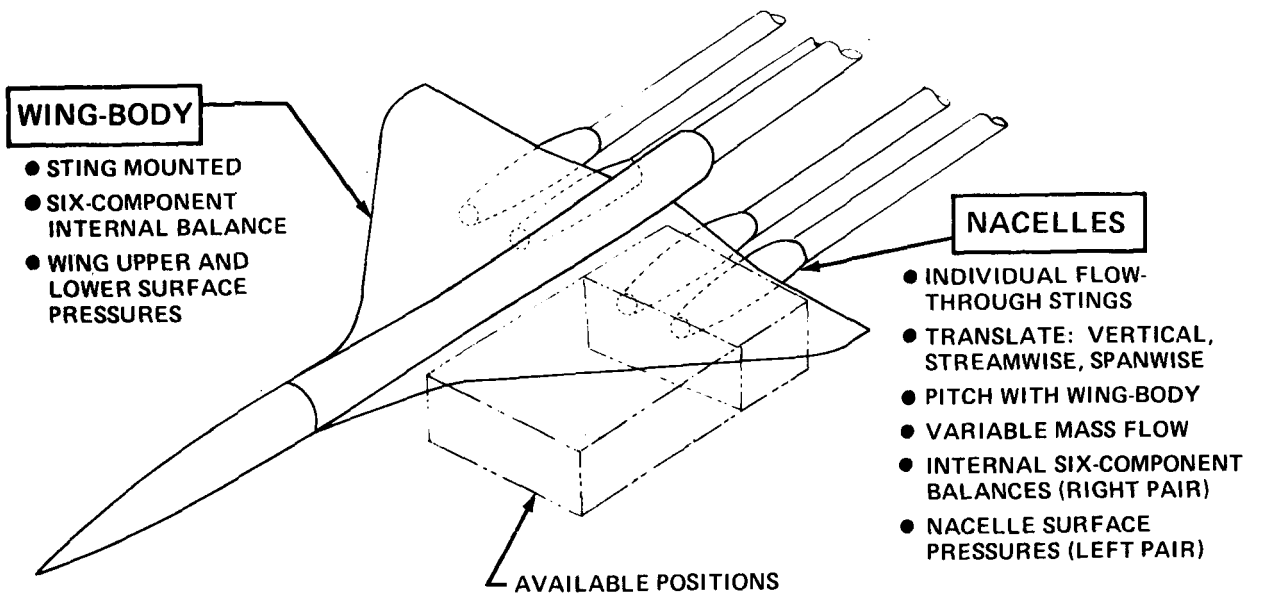
Figure 1.- NASA–Ames nacelle/airframe interference model features.

WING-BODY GEOMETRY

75.0 deg
50.5 deg
0.024-SCALE MODEL

NACELLE DETAILS

INTERNAL LIP SURFACE ON BALANCE
BALANCE FLEXURE FITTING
NACELLE EXTERNAL CONTOUR
NACELLE STING

WING PRESSURE LOCATIONS

X
Y

- Upper and lower surface
- Lower surface only

NACELLE PRESSURE STATIONS

6.14 deg
9.74 deg
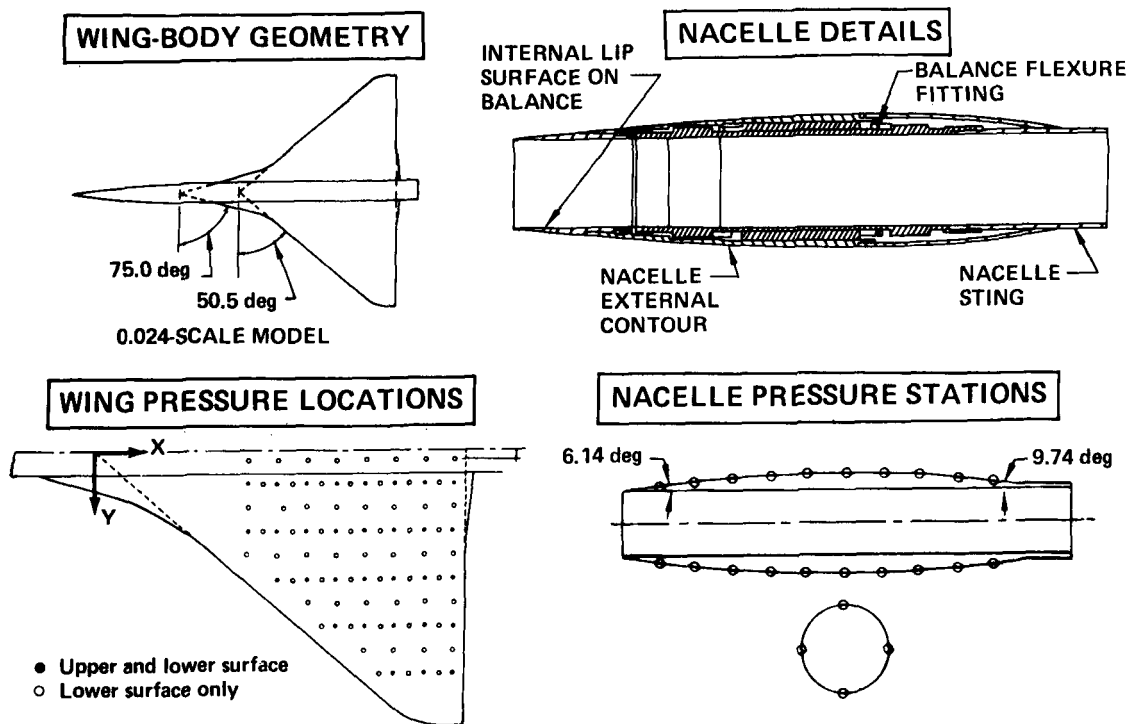
Figure 2.- Wind tunnel model details.

185

TYPICAL SUPERSONIC NACELLE INSTALLATION

INBOARD WING

OUTBOARD WING

WIND TUNNEL MODEL NACELLE AT SAME SCALE

WING CHORD PLANE AT OUTBOARD NACELLE

TRAILING EDGE (STATION 5)

6.14 deg

9.74 deg

₵
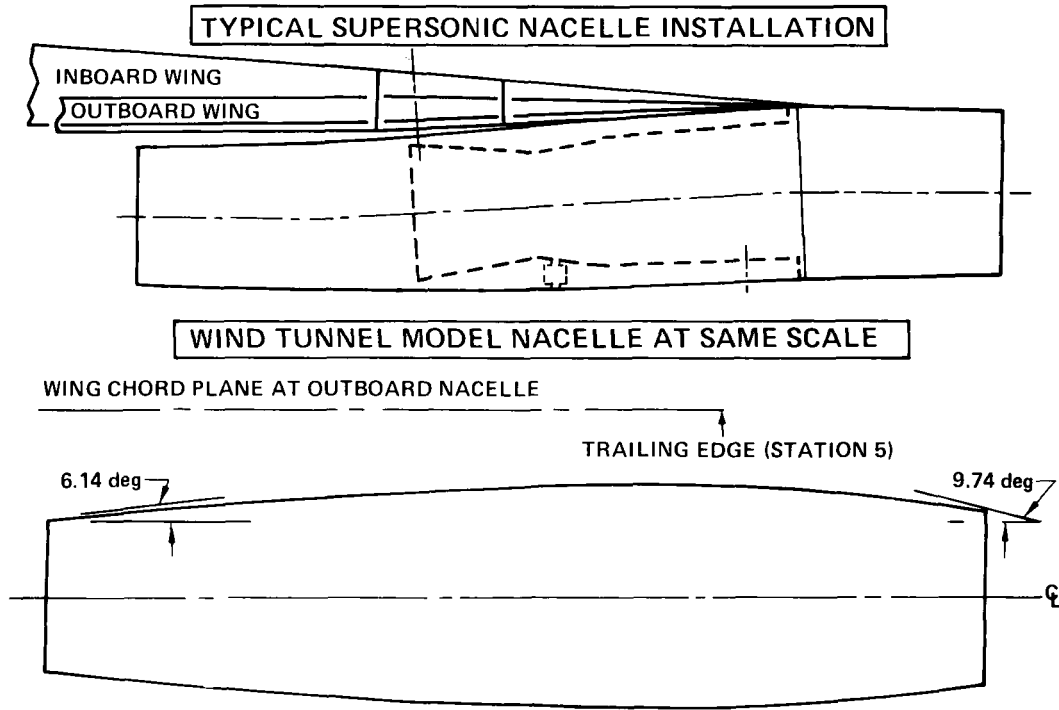
Figure 3.- Nacelle geometry comparison.

THIS PAPER
● MACH EFFECTS
● ANGLE OF ATTACK EFFECTS
● SPILLAGE EFFECTS
● NACELLE STATION

①②③④⑤⑥
NACELLE STATION

● THREE DIFFERENT NACELLE SPANWISE LOCATIONS

NO STAGGER

ONE-STATION STAGGER

TWO-STATION STAGGER
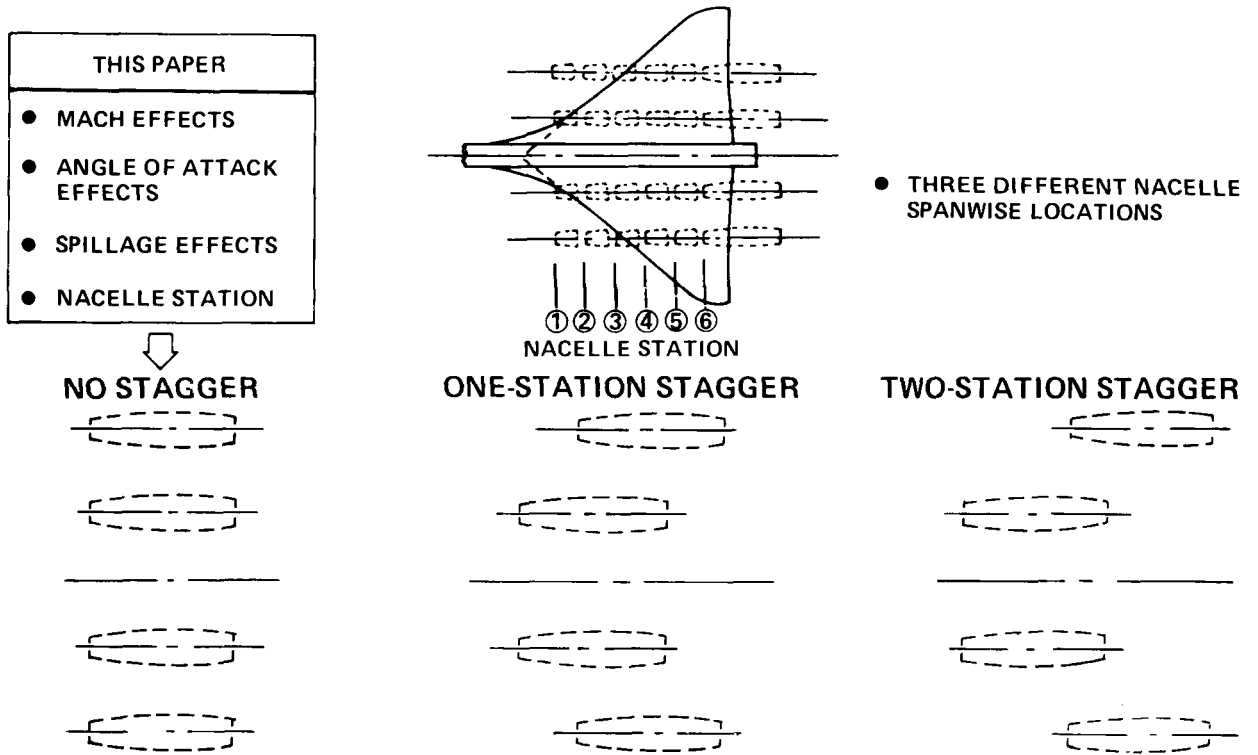
Figure 4.- Tested nacelle locations.

186

| DRAG COMPONENT | METHOD [a] | NACELLE PRESSURE FIELD REPRESENTATION | | | | |
| | | INLET MACH NUMBER | | THEORY | PRESSURE FIELD SUPERPOSITION | |
		M_∞	M_{LOC}		"WRAP"	"GLANCE"
C_{D_F}–FRICTION DRAG	●SOMMER AND SHORT T* METHOD	●	X	——	——	——
C_{D_W}–VOLUME WAVE DRAG	●FAR-FIELD THEORY (AREA RULE) PROGRAM	●		LINEAR	●	
	●NEAR-FIELD THEORY PROGRAM	●		"WHITHAM"	●	●
C_{D_L}–DRAG DUE TO LIFT	●LIFT ANALYSIS PROGRAM	●	X	"WHITHAM"	●	●

X—CAPABILITY

●—USED IN THIS STUDY

[a] MIDDLETON/CARLSON–SUPERSONIC AERODYNAMIC DESIGN AND ANALYSIS SYSTEM

Figure 5.– Drag prediction methods.

"WRAP" APPROACH

NACELLE CENTERLINES

●SHOCKS AND PRESSURE "WRAP" AROUND NACELLES ADJACENT TO OUTER WING
●FAR-FIELD APPROACH

"GLANCE" APPROACH

NACELLE CENTERLINES

●SHOCKS AND PRESSURES "GLANCE" AWAY FROM WING AT ADJACENT NACELLES
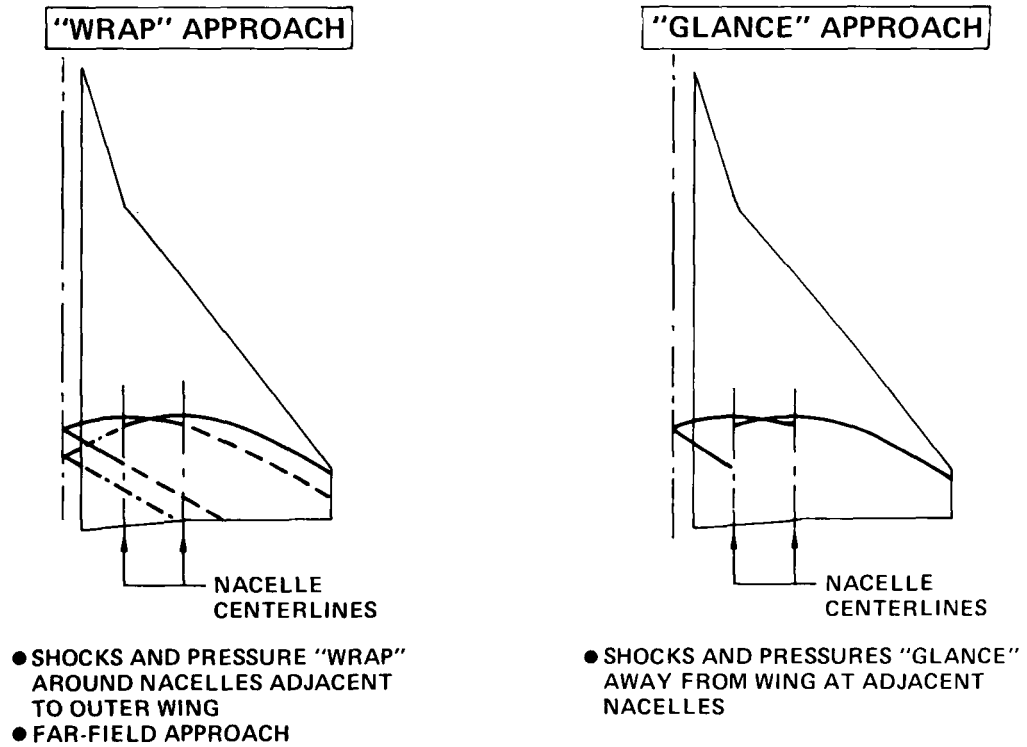
Figure 6.– "Glance" and "wrap" pressure fields superposition.

NACELLE
INSTALLED = | FRICTION DRAG | + | WAVE DRAG | + | LIFT INTERFERENCE |
DRAG

                                         ‖   ‖
                                NACELLE PRESSURE DRAG   CHANGE IN WING-BODY
                                                            DRAG DUE TO LIFT

                                         +   NACELLE ON WING LIFTING
                                NACELLE ON WING-BODY   SURFACE
         NACELLE SKIN   VOLUME
         FRICTION
                                         +   +

                                WING-BODY VOLUME   WING LIFTING PRESSURES
                                   ON NACELLE   ON NACELLES

                                         +
                                MUTUAL NACELLE
                                 INTERFERENCE
                                ●ADJACENT ●OFF WING
                                            ON-TO
                                            NACELLE
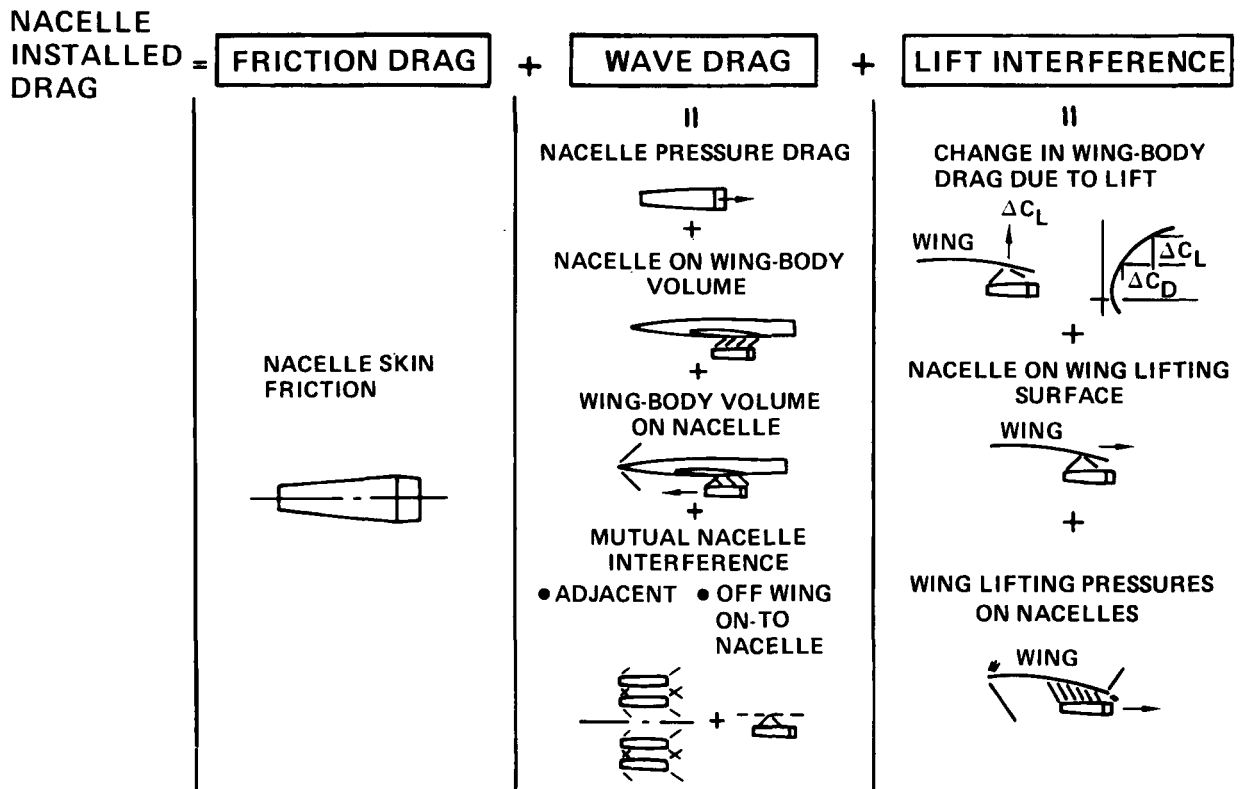
Figure 7.- Nacelle installed drag components — no spillage.
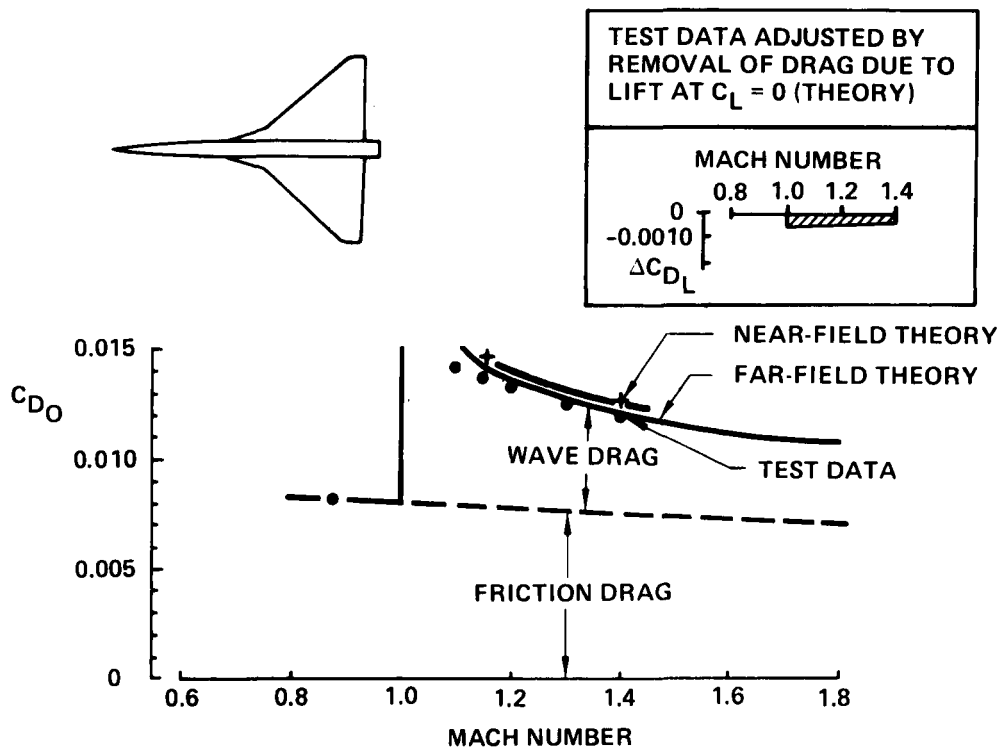
Figure 8.- Wing + body drag comparisons at zero lift.

188
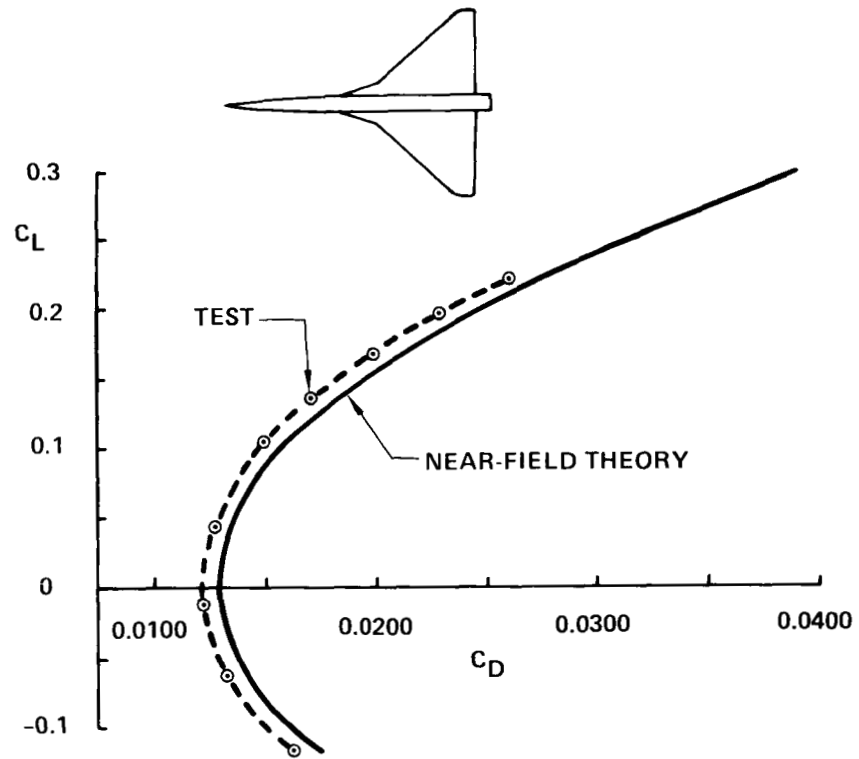
Figure 9.- Wing + body drag polar — mach 1.4.
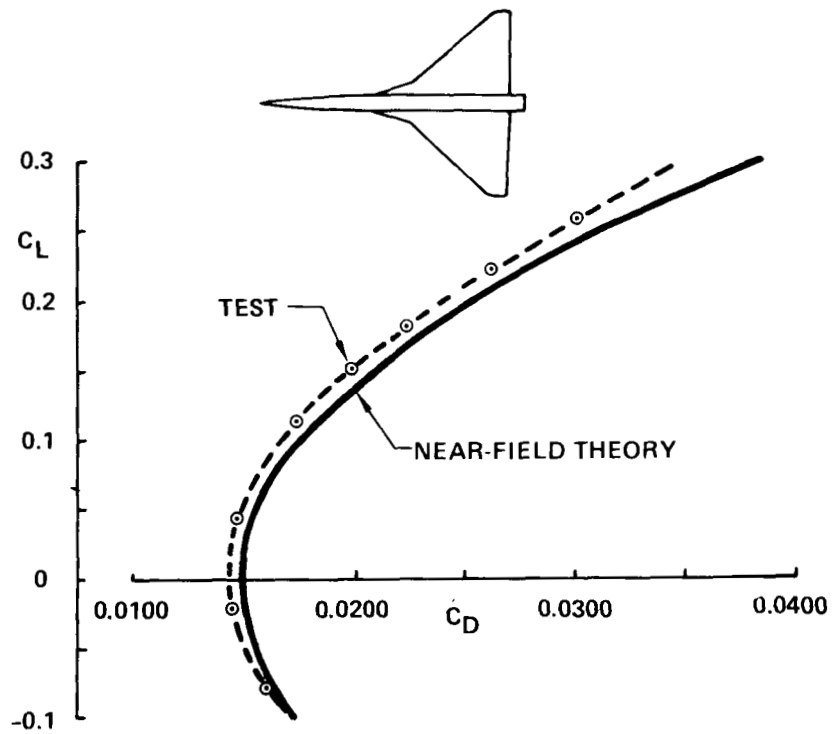
Figure 10.- Wing + body drag polar — mach 1.15.
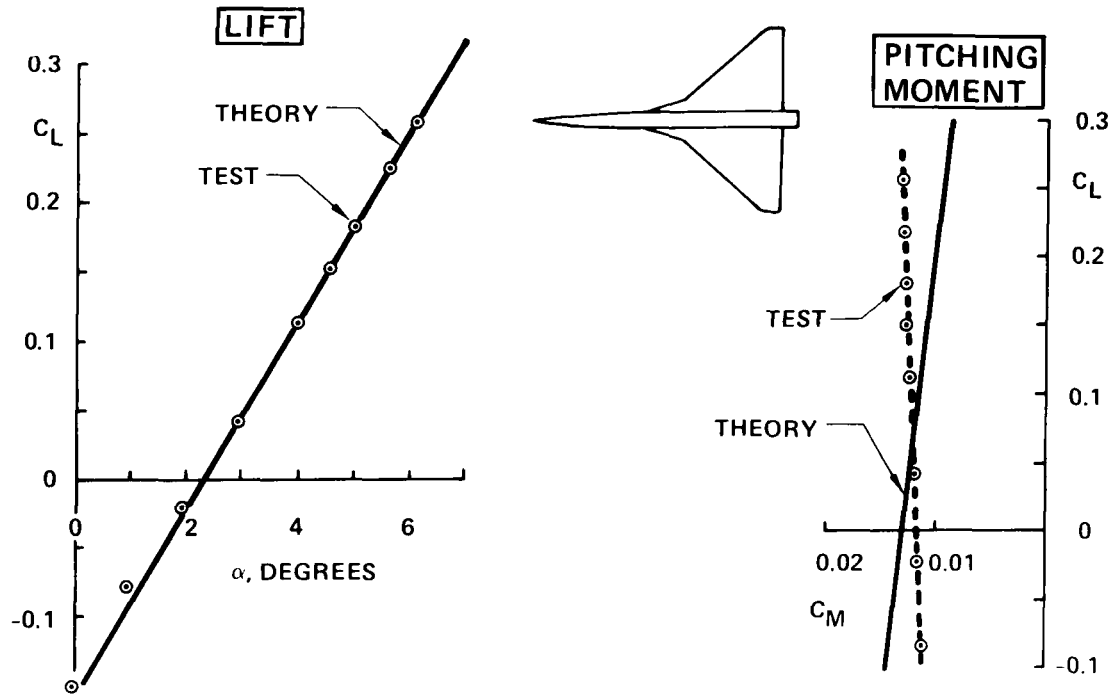
Figure 11.— Wing + body lift and pitching moment curves — M = 1.4.
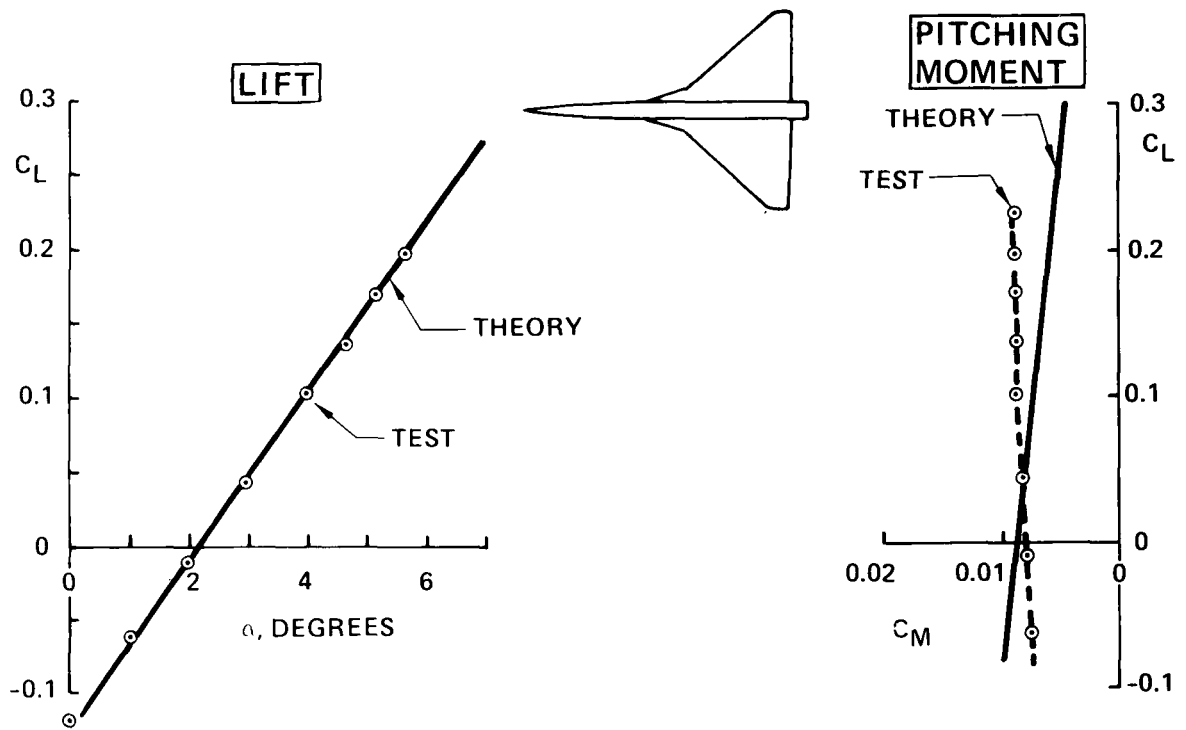
Figure 12.— Wing + body lift and pitching moment curves — M = 1.15.
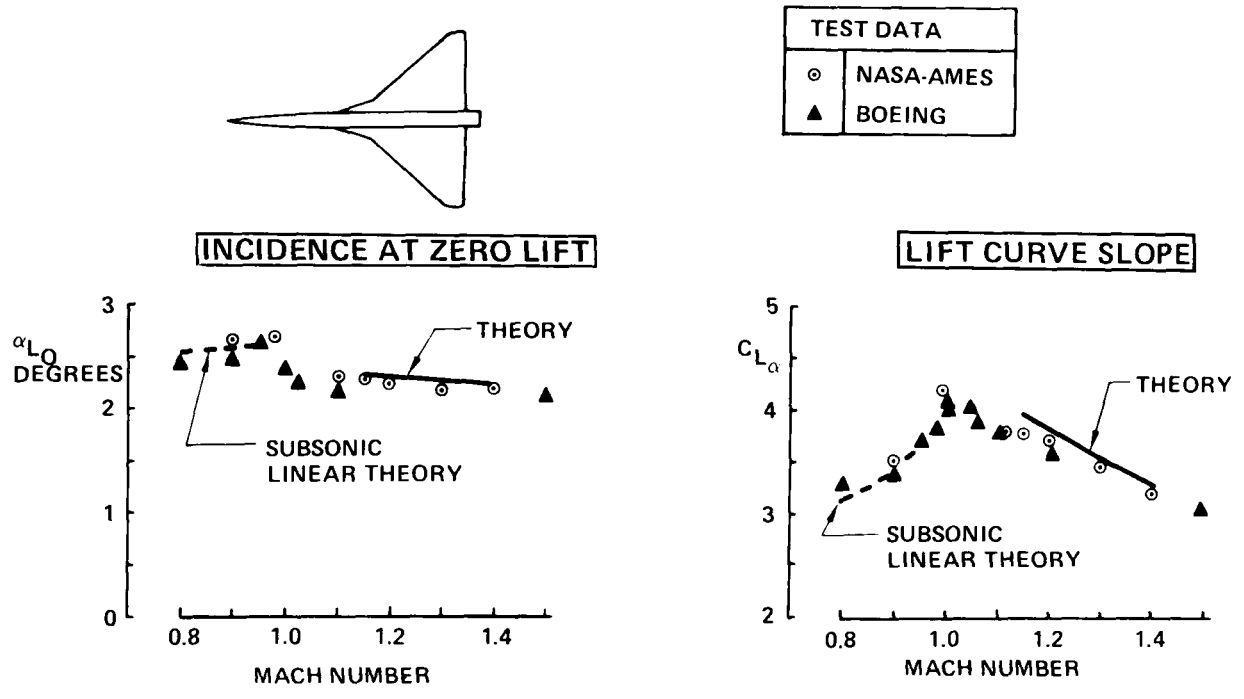
Figure 13.- Wing + body lift characteristics.
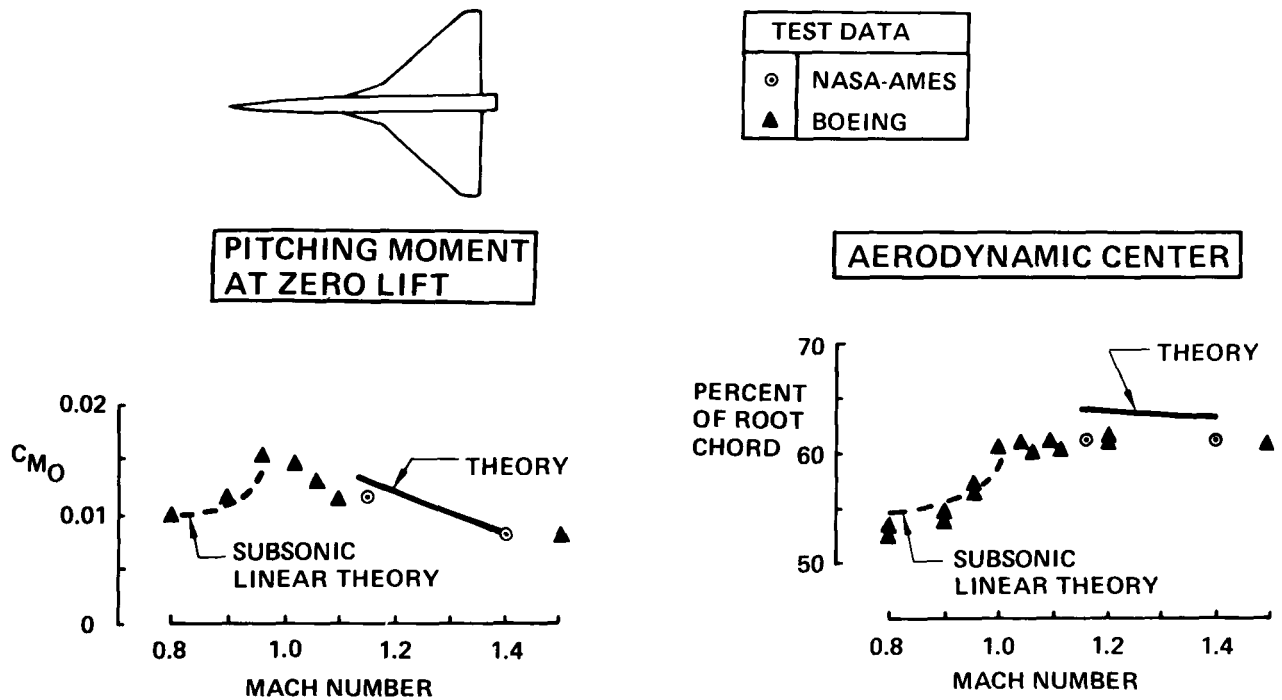
Figure 14.- Wing + body pitching moment characteristics.

Figure 15.- Isolated nacelle zero-lift comparisons.

Figure 16.- Nacelle interference pressure fields, M = 1.4; aft nacelle location — station 5.
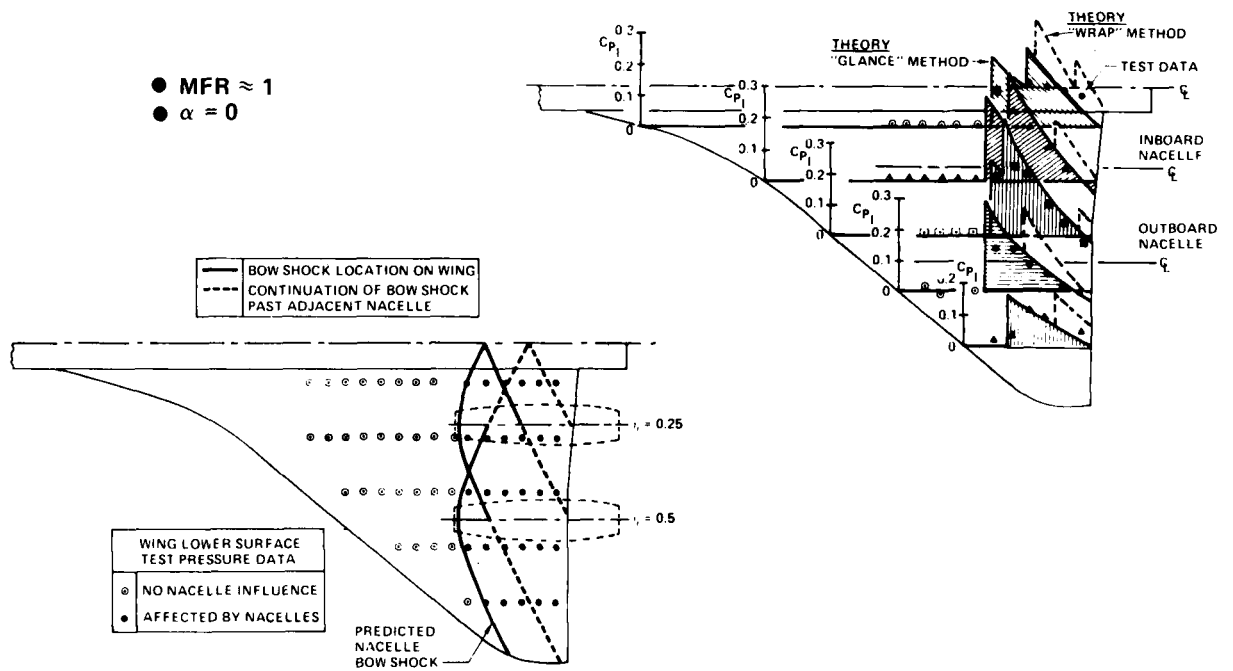
Figure 17.- Nacelle interference pressure fields, M = 1.15;
aft nacelle location — station 5.
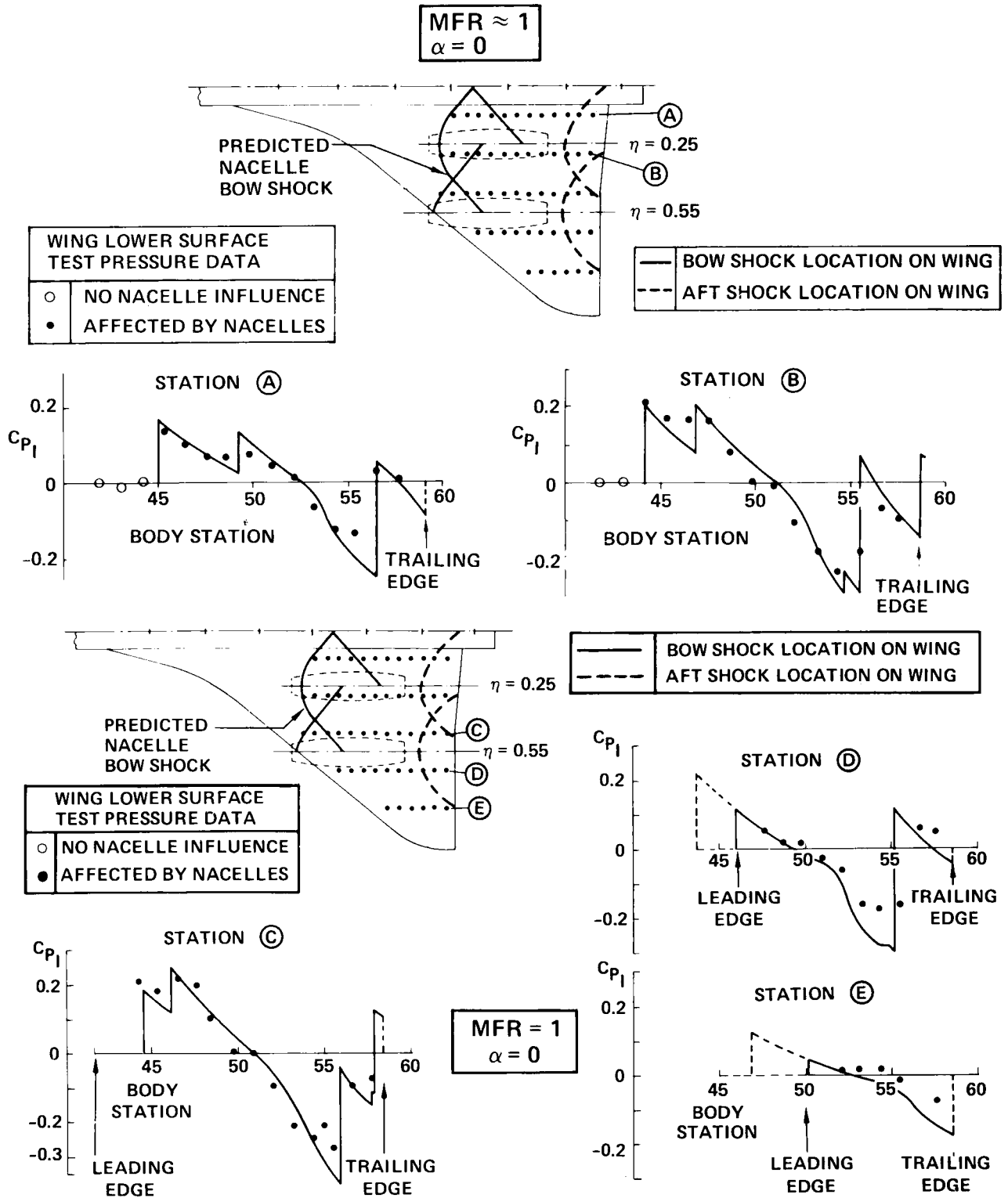
Figure 18.- Nacelle interference pressure fields — M = 1.4; forward location — station 3.
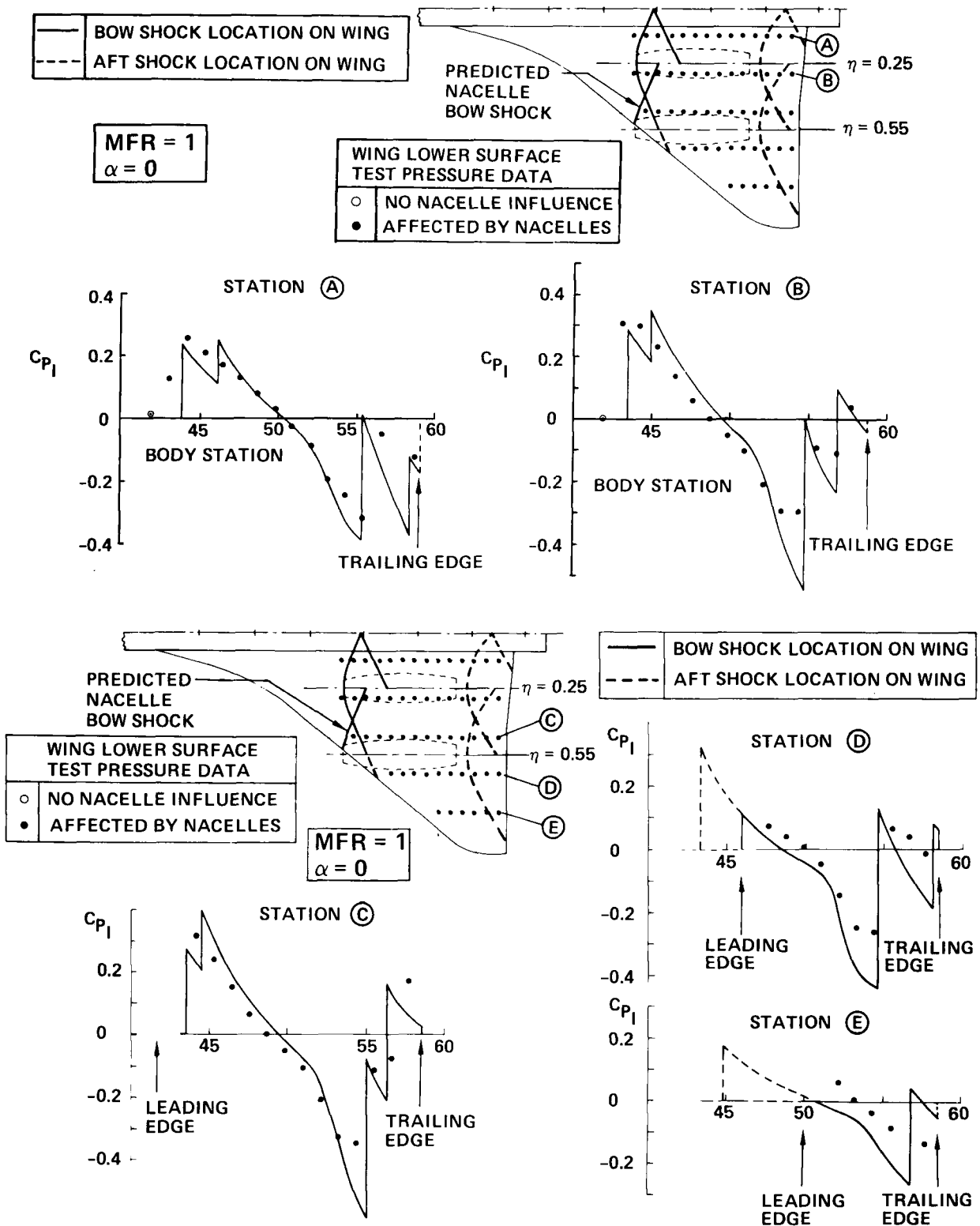
Figure 19.- Nacelle interference pressure fields — M = 1.15;
forward nacelle location — station 3.

TEST DATA	
⊙	INTERFERENCE ON WING-BODY
△	TOTAL NACELLE CONTRIBUTION

MFR ≈ 1

η = 0.25

η = 0.55

PITCHING MOMENT

Δc_M

THEORY —

-0.01

-0.01   0   0.10   0.20 c_L 0.30

Δc_L

LIFT

THEORY —

0.06

0.04

0.02

0

0   2   4   6   8

α, DEGREES

DRAG

Δc_D

TOTAL NACELLE INSTALLED DRAG

THEORY
TEST

ISOLATED NACELLES

0.0040

0.0020

c_{D_W}

c_{D_F}

-0.10   0.10   0.20   0.30 c_L

-0.0040

NACELLE INTERFERENCE ON WING + BODY

TEST

THEORY
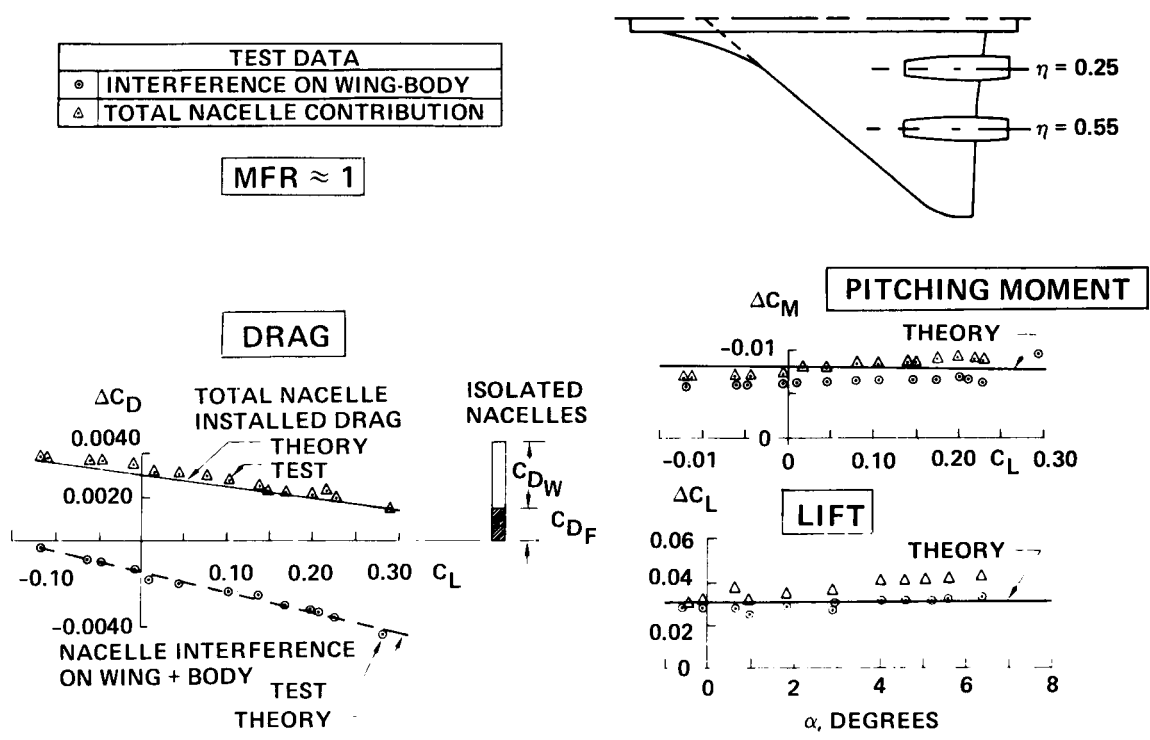
Figure 20.- Nacelle contribution to lift, drag, and pitching moment —
M = 1.4.

η = 0.25

η = 0.55

(x/c) OUTBOARD = 0.508

TEST DATA	
⊙	INTERFERENCE ON WING-BODY
△	TOTAL NACELLE CONTRIBUTION

MFR ≈ 1.0

PITCHING MOMENT

-0.015

-0.005

THEORY

Δc_M

-0.1   0   0.1   0.2   0.3

c_L

TOTAL NACELLE INSTALLED DRAG

Δc_D

THEORY
TEST

ISOLATED NACELLES

c_{D_W}

c_{D_F}

0.0020

0.1   0.2 c_L 0.3

-0.0040

TEST
THEORY

NACELLE INTERFERENCE ON WING-BODY

LIFT

0.06

Δc_L

0.02

THEORY

0   2   4   6   8

α, DEGREES
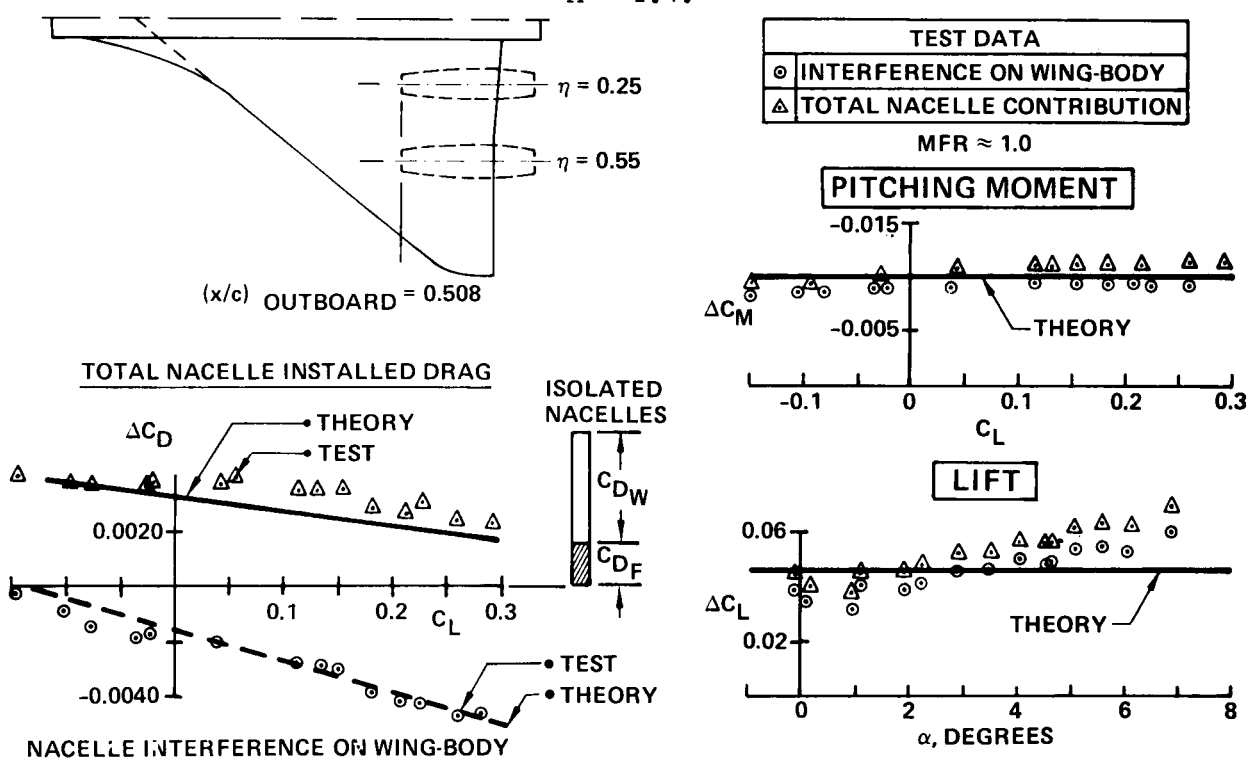
Figure 21.- Nacelle contribution to lift, drag, and
pitching moment — M = 1.15.

196

$$\Delta C_L = \frac{L}{q S_R} = \frac{2 \Delta S}{\beta S_R}$$

$$\frac{(\Delta C_L)_{CP}}{(\Delta C_L)_{C_P = 0}} = \frac{\beta_\infty \, q_\ell}{\beta_\ell \, q_\infty} = \left[0.7 \, C_p \, M_\infty^2 + 1 \right] \left(\frac{M_\ell}{M_\infty} \right)^2 \left(\frac{\beta_\infty}{\beta_\ell} \right)$$

$$M_\ell = \sqrt{5 \left[\frac{1 + 0.2 \, M_\infty^2}{\left\{ 0.7 \, C_p \, M_\infty^2 + 1 \right\}^{1/3.5}} - 1 \right]}$$
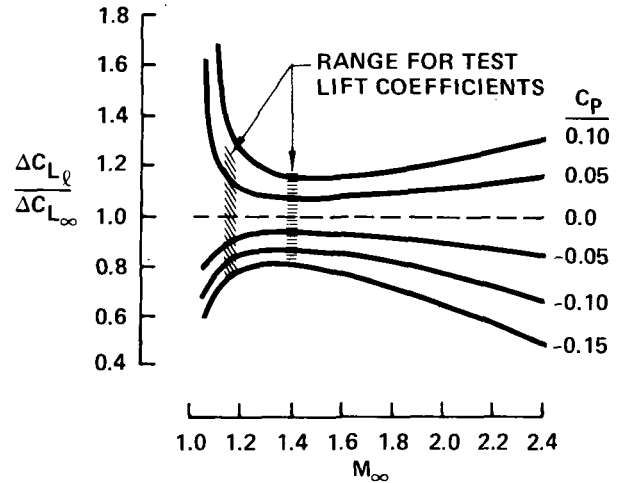
Figure 22.- Effect of local pressure field on interference lift.
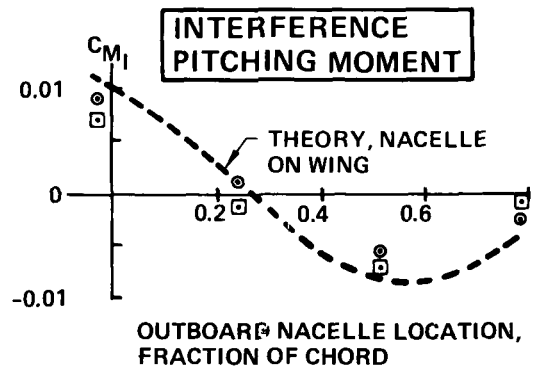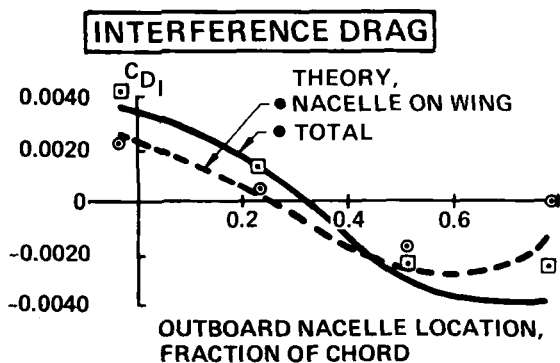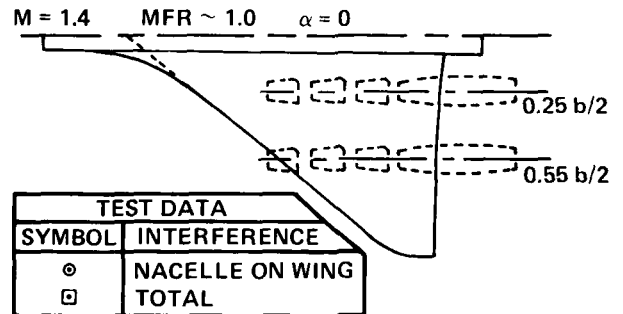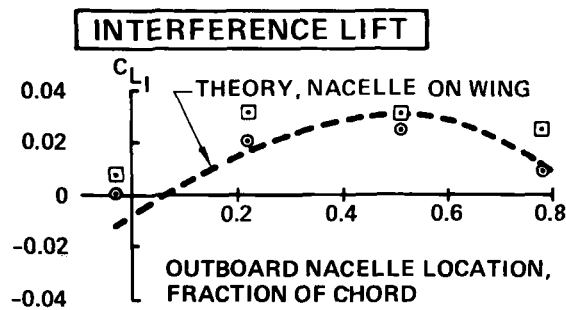
Figure 23.- Effect of nacelle locations on aerodynamic interference —
M = 1.4.

197

M = 1.15 MFR ~ 1.0 α = 0

INTERFERENCE LIFT

c_{L_i}

0.10

0.05

0

-0.05

THEORY, NACELLE ON WING

0.2   0.4   0.6   0.8

OUTBOARD NACELLE LOCATION,
FRACTION OF CHORD

0.25 b/2

0.55 b/2

TEST DATA	
SYMBOL	INTERFERENCE
⊙	NACELLE ON WING
⊡	TOTAL

INTERFERENCE DRAG

c_{D_i}

0.0100

0.0050

0

-0.0050

THEORY, NACELLE ON WING

TOTAL

0   0.2   0.6

OUTBOARD NACELLE LOCATION,
FRACTION OF CHORD

INTERFERENCE PITCHING MOMENT

c_{M_i}

0.020

0.010

-0.010

THEORY,
NACELLE ON WING

0   0.2   0.4   0.6

OUTBOARD NACELLE LOCATION,
FRACTION OF CHORD

Figure 24.- Effect of nacelle location on aerodynamic interference —
M = 1.15.

APPROACH:

●USE MOECKEL'S METHOD TO PREDICT
NORMAL SHOCK LOCATION

●USE SIMPLE POLYNOMIAL REPRE-
SENTATION OF STREAMTUBE SHAPE

●CHECK STREAMTUBE REPRESENTA-
TION

　●NACELLE PRESSURES
　●NACELLE FORCES

HYPERBOLIC
SHOCK

SONIC LINE

CAPTURE STREAMTUBE EQUATION

NORMAL
SHOCK

r_s

X

₵

CAPTURE
STREAMTUBE

$$\frac{r_s}{R_i} = \sqrt{MFR} + \left(1 - \sqrt{MFR}\right)\left(1 - \left|\frac{X}{L_s}\right|^N\right)$$

MFR =	CAPTURE AREA
	INLET AREA

QUADRATIC REPRESENTATION: N = 2

L_s

SHOCK
STANDOFF
DISTANCE
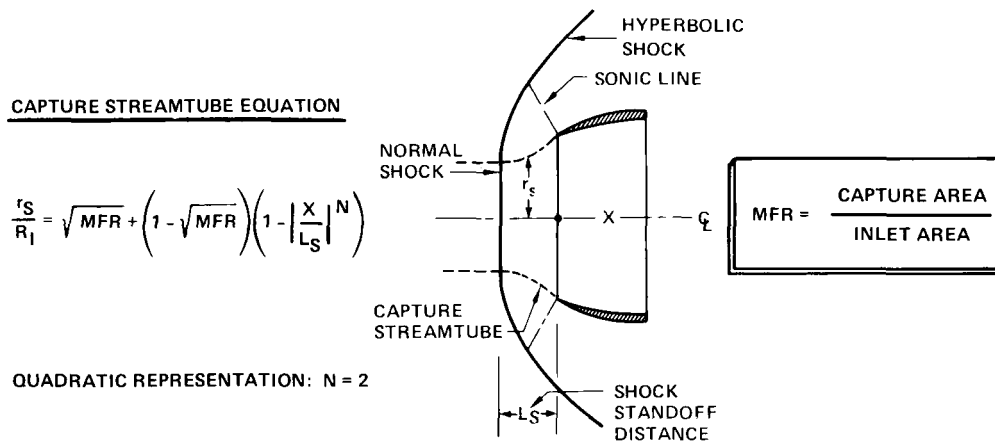
Figure 25.- Spillage streamtube representation.
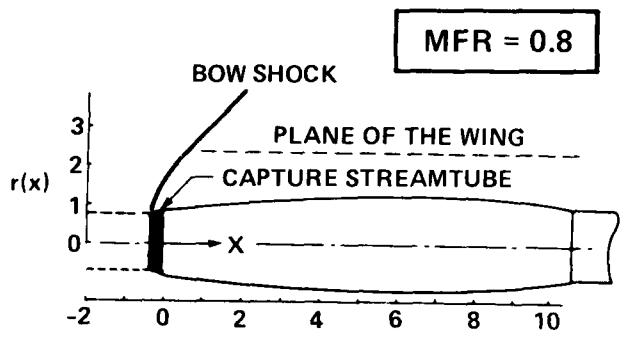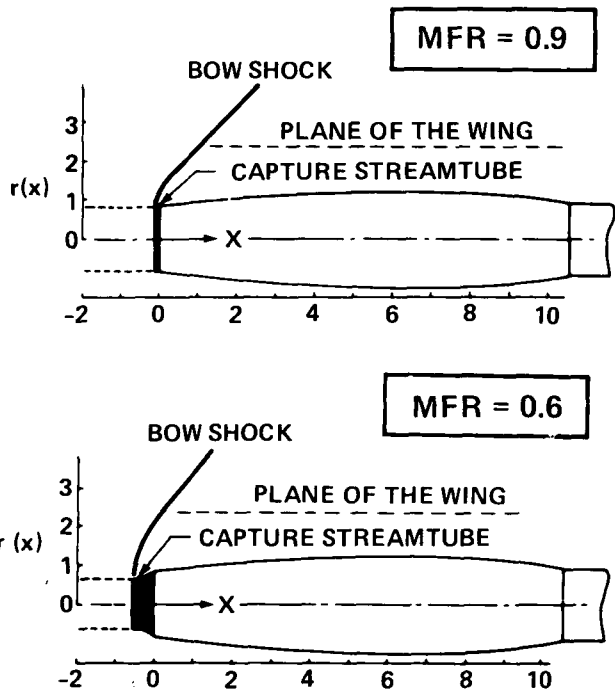
Figure 26.- Calculated streamtube shapes — M = 1.4.
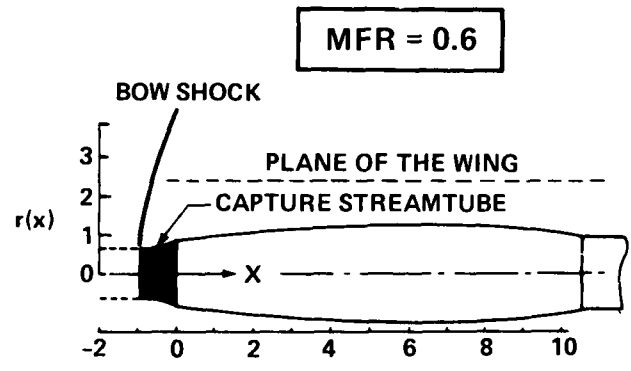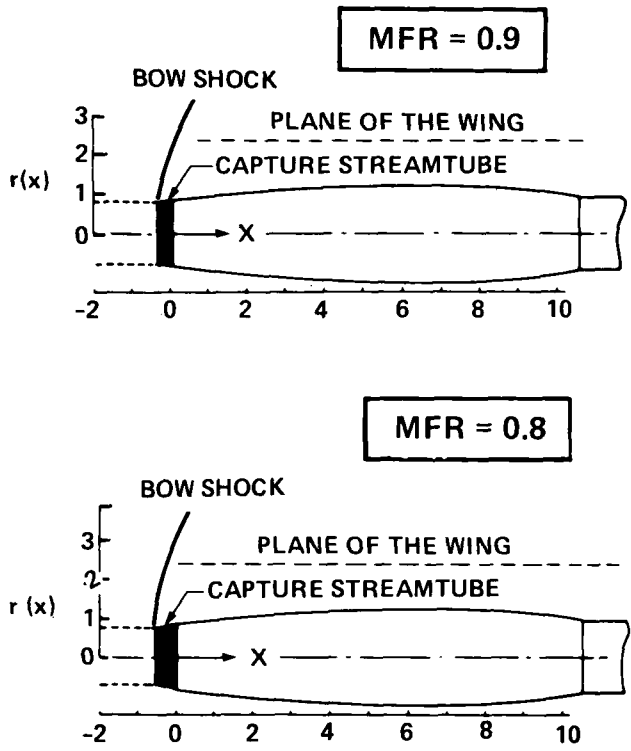
Figure 27.- Calculated streamtube shapes — M = 1.15.
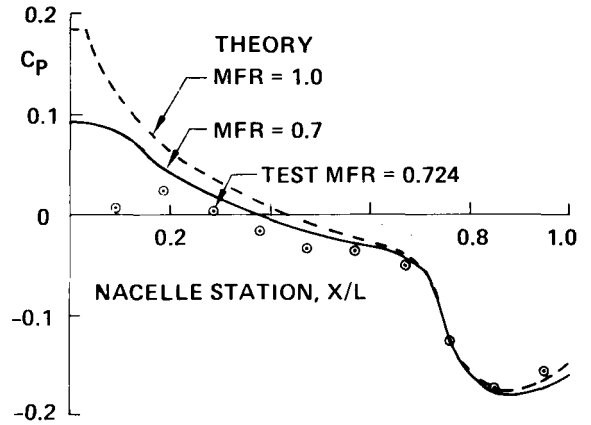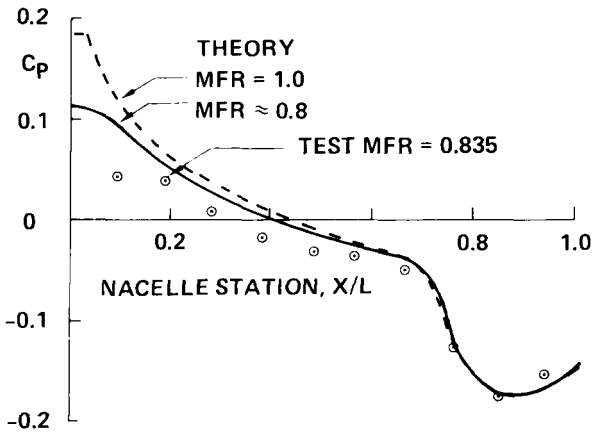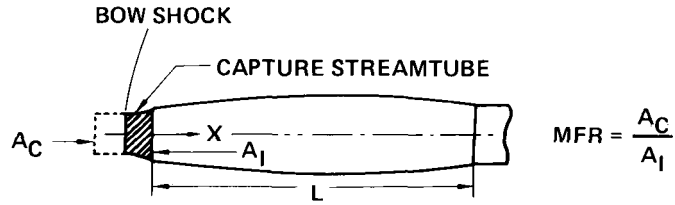
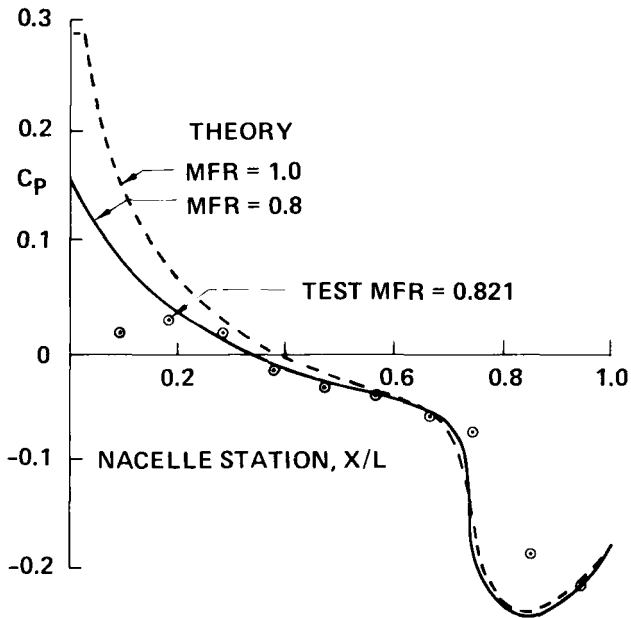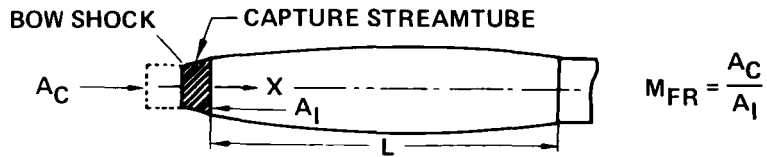Figure 28.- Effect of spillage on isolated nacelle pressures — M = 1.4.
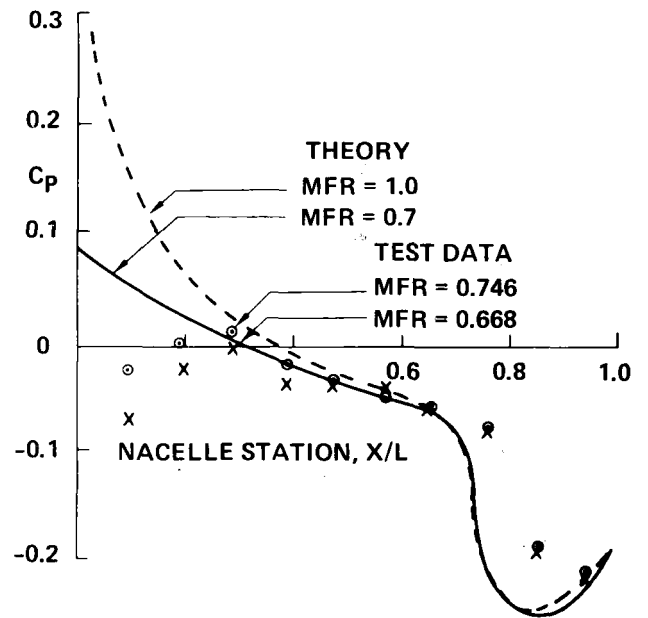
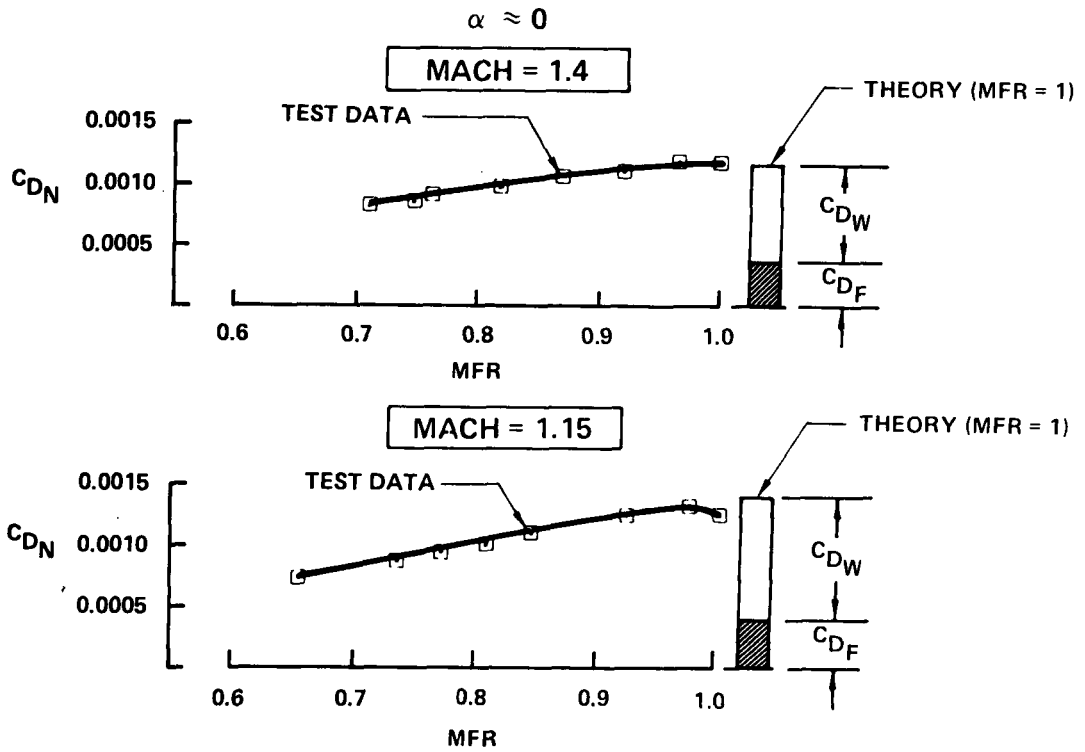Figure 29.- Effect of spillage on isolated nacelle pressures — M = 1.15.

200

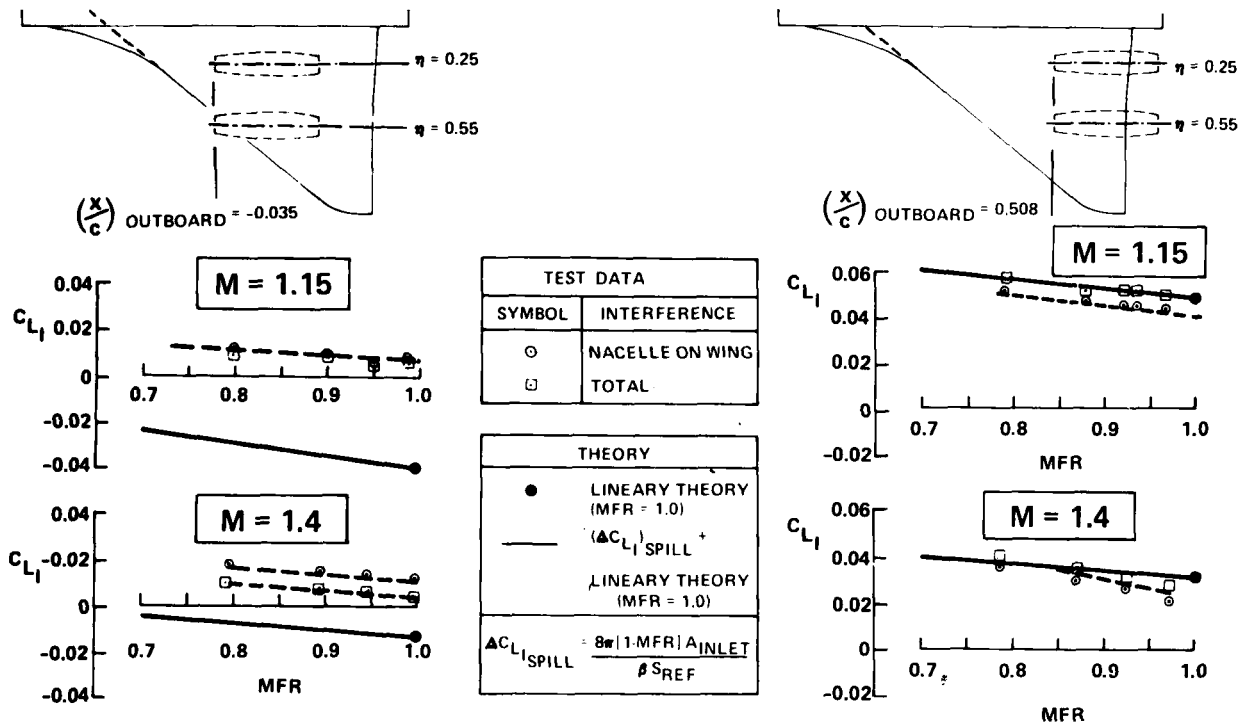Figure 30.- Effect of spillage on isolated nacelle drag.

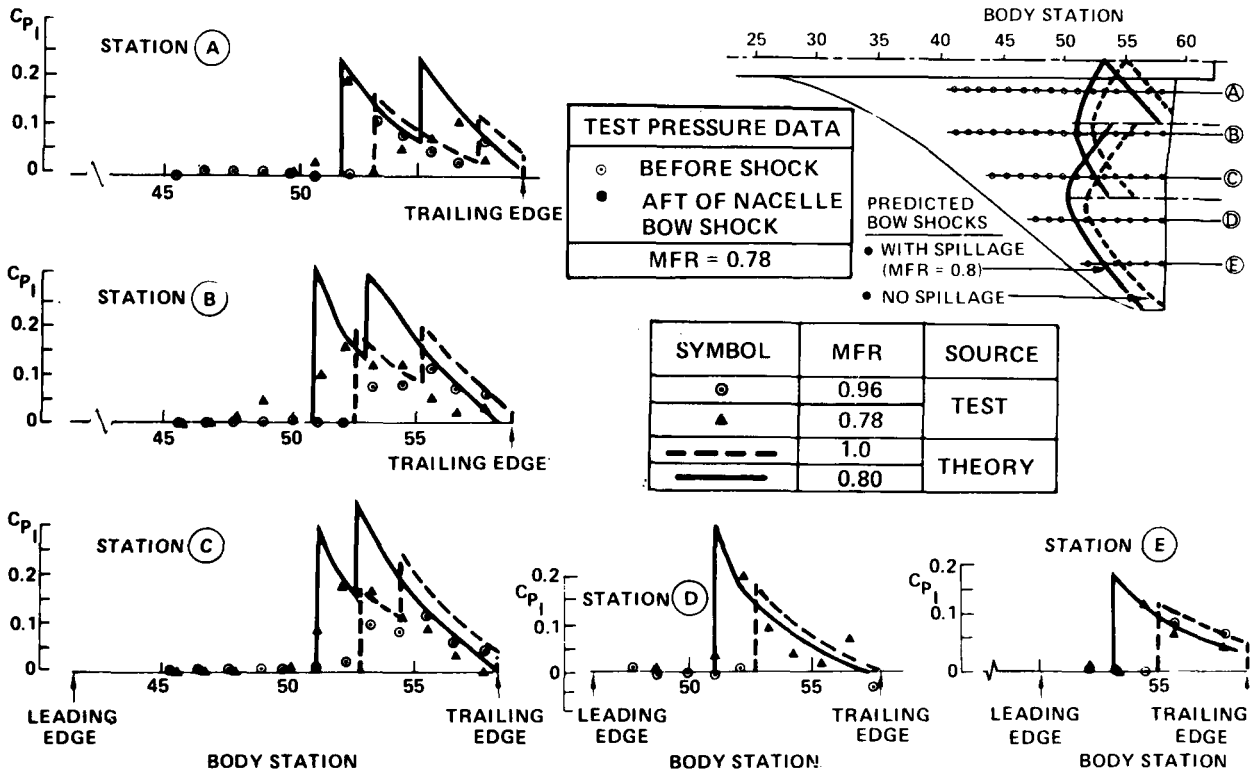Figure 31.- Slender body theory estimates spillage interference lift.

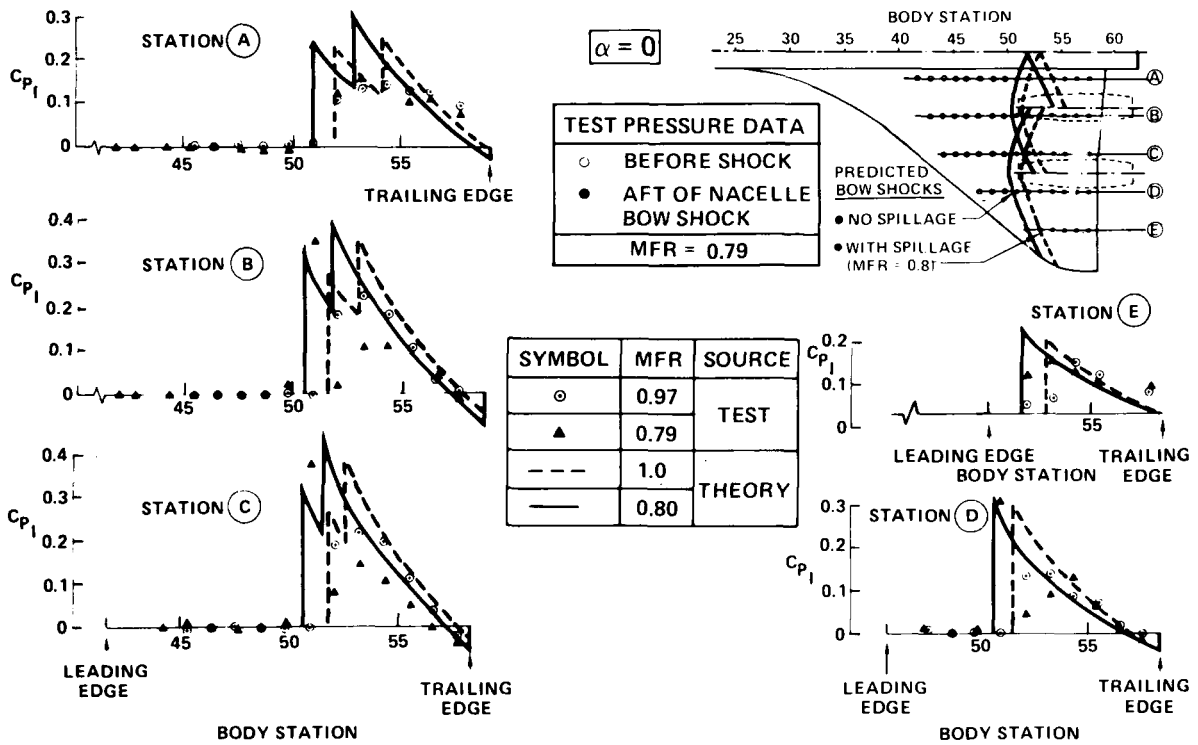Figure 32.- Effect of nacelle spillage on interference pressures — M = 1.4.

Figure 33.- Effect of nacelle spillage on interference pressures — M = 1.15.
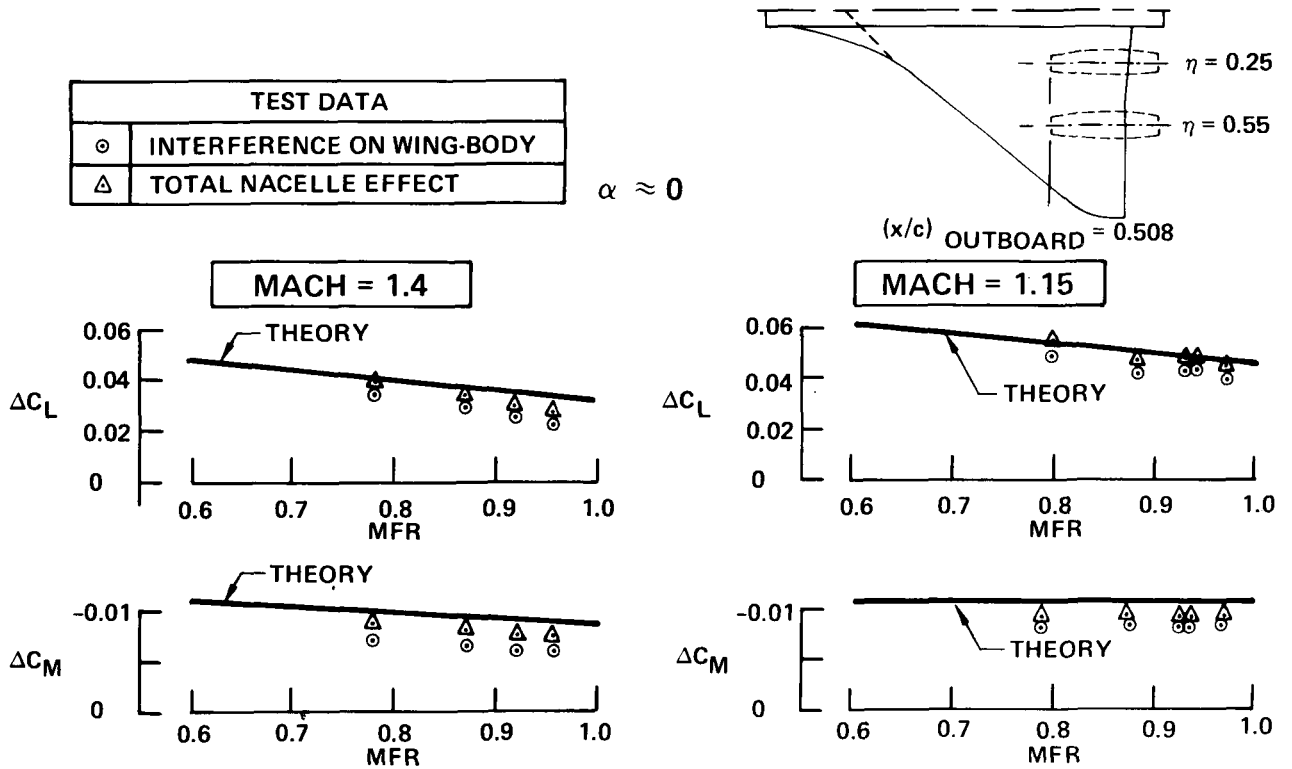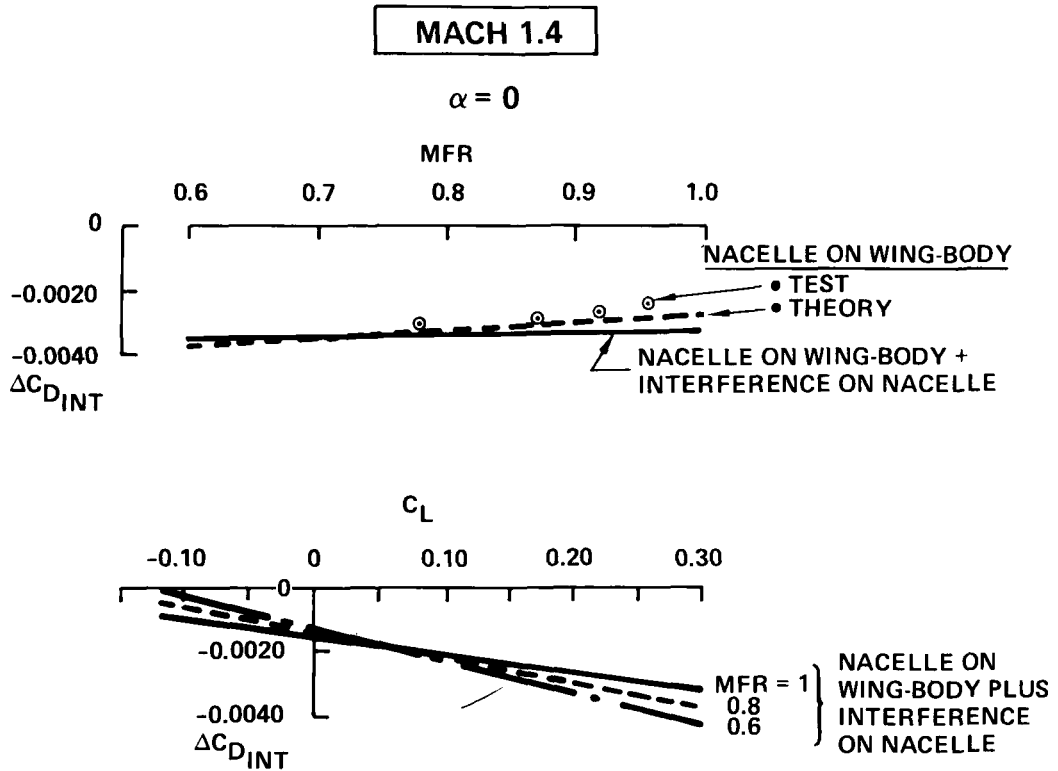
Figure 34.- Effect of spillage on lift and pitching moment.

Figure 35.- Spillage effects on nacelle interference.